FEBRUARY 2021 M.Sc. in Electrical and Electronics Engineering MUHAMMED AKIL RIHAVI

REPUBLIC OF TURKEY

GAZIANTEP UNIVERSITY

GRADUATE SCHOOL OF NATURAL & APPLIED SCIENCES

DEVELOPMENT OF MAXIMUM POWER POINT TRACKING SYSTEM (MPPT) FOR SOLAR PANEL

M.Sc. THESIS

IN

ELECTRICAL AND ELECTRONICS ENGINEERING

BY

MUHAMMED AKIL RIHAVI

FEBRUARY 2021

DEVELOPMENT OF MAXIMUM POWER POINT TRACKING SYSTEM (MPPT) FOR SOLAR PANEL

M.Sc. Thesis

in

Electrical and Electronics Engineering

Gaziantep University

Supervisor

Prof. Dr. Ergun ERÇELEBİ

by

Muhammed Akil RIHAVI

February 2021

I hereby declare that all information in this document has been obtained and presented in accordance with academic rules and ethical conduct. I also declare that, as required by these rules and conduct, I have fully cited and referenced all material and results that are not original to thiswork.

Muhammed Akil RIHAVI

ABSTRACT

DEVELOPMENT OF MAXIMUM POWER POINT TRACKING SYSTEM (MPPT) FOR SOLAR PANEL

RIHAVI, Muhammed Akil
M.Sc. in Electrical and Electronics Engineering
Supervisor: Prof. Dr. Ergun ERÇELEBİ
February 2021
62 Pages

Due to the global energy crisis and environmental problems, the utilization of photovoltaic (PV) systems as an electric source has increased exponentially. It is expected that this usage trend will keep increasing in the near future too. However, the output power from the photovoltaic modules is affected by radiation intensity of the solar cells. Therefore, to exploit all power of photovoltaic panel and maximize the efficiency of the photovoltaic (PV) systems, it is necessary to track the maximum power point of the input source. In the thesis, the efficiency of perturb and observe (P and O) maximum power point tracker (MPPT) has been enhanced. The efficiency improving has been achieved by ameliorating the tracking speed (transient response) and decreasing the steady state oscillation. A step-size perturbation is utilized to decrease the oscillation and minimize the reaching time of operating point to MPPT. When the operating point is far from the MPPT, the perturbation is made larger to ensure that the tracking speed is maximized. But as the operating point gets closer to the MPPT, the perturbation reduces. The algorithm proposed for maximum power point tracking system (MPPT) for solar panel has been realized on boost converter by design of electronic card having STM32 microcontroller. The card scans the gained power of PV panel over short periods to adapt the nonlinear electrical characteristics of PV panel. Extensive experimental and simulation results have shown that the proposed algorithm is effective in variable weather conditions.

Key Words: Photovoltaic (PV) Systems, P and O Algorithm, MPPT, Boost Converter, Renewable Energy.

ÖZET

GÜNEŞ PANELİ İÇİN MAKSİMUM GÜÇ NOKTASİ TAKİP SİSTEMİNİN GELİŞTİRİLMESİ

RIHAVI, Muhammed Akil
Yüksek Lisans Tezi, Elektrik-Elektronik Mühendisliği
Danışman: Prof. Dr. Ergun ERÇELEBİ
Şubat 2021
62 Sayfa

Küresel enerji krizi ve çevre sorunları nedeniyle, fotovoltaik (FV) sistemlerin elektrik kaynağı olarak kullanımı katlanarak artmaktadır. Bu büyümenin yakın gelecekte de devam etmesi beklenmektedir. Ancak, fotovoltaik modüllerin çıkış gücü güneş hücrelerinin radyasyon yoğunluğundan etkilenmektedir. Bu nedenle, fotovoltaik panelin tüm gücünden faydalanmak ve fotovoltaik (PV) sistemlerin verimliliğini en üst düzeye çıkarmak için, giriş kaynağının maksimum güç noktasını takip etmek gerekmektedir. Tezde, karışıklık ve gözlemleme (K ve G) maksimum güç noktası izleyicisinin (MGNİ) verimliliği artırılmıştır. İzleme hızının iyileştirilmesi (geçici yanıt) ve kararlı durum salınımının azaltılmasıyla verimlilik artışı sağlanmıştır. Salınımı azaltmak ve çalışma noktasının MGNİ'ye ulaşma süresini en aza indirmek için adım boyutunda bir karışıklık kullanılmaktadır. Çalışma noktası MGNİ 'den uzak olduğunda, izleme hızının en üst düzeye çıkarılmasını sağlamak için karışıklık büyütülmektedir. Ancak, çalışma noktası MGNİ'ye yaklaştıkça karışıklık azalmaktadır. Güneş paneli için maksimum güç noktası takip sistemi için önerilen algoritma, STM32 mikro denetleyiciye sahip elektronik kart tasarımı ile artırıcı dönüştürücü üzerinde gerçekleştirilmiştir. Kart, FV panelin doğrusal olmayan elektriksel özelliklerini uyarlamak için kısa sürelerde FV panelin kazandığı gücü taramaktadır. Kapsamlı deneysel ve benzetim sonuçları, önerilen algoritmanın değişken hava koşullarında etkili olduğunu göstermiştir.

Anahtar Kelimeler: Fotovoltaik (FV) Sistemler, K ve G Algoritması, MGNİ,

Artırıcı Dönüştürücü, Yenilenebilir Enerji.

To my parents and my lovely wife.

ACKNOWLEDGEMENTS

In the name of Allah, the Most Gracious, the Most Merciful. I would like to start by thanking Allah for giving me this opportunity to fulfill my dream to pursue Masters.

I would like to acknowledge and express my sincere gratitude to my supervisor Prof. Dr. Ergun ERÇELEBİ for giving me the opportunity to do Master's thesis under his supervision and providing me with continued support during my research. His immense knowledge, continuous strives to keep me at course and senses of quality in research have been of inestimable help through the time of research and for writing this thesis.

Secondly, I would be not here without the continued support of my role model, my Dad, my ever-loving mom, my dear wife, and my family members. I love you all! I would also like to thank Eng. Mohamad Wael Zakkor, Eng. Ahmad Baida, and Abdulatif Karem. Thank you for your supportive suggestions and commendable help. Thank you for being here, whenever I need you.

Finally, I would like to express my appreciation to the TURKEY SCHOLARSHIP COMMITTEE for granting me this scholarship to pursue my Masters in Turkey.

TABLE OF CONTENTS

LIST OF TABLES

Page

LIST OF FIGURES

Page

LIST OF SYMBOLS

α	Constant relationship between I_{mp} and $P_{m.}$
F_s	Switching frequency.
I_d	Current in the P -N junction of the PV cell.
I_g	Current generated due to photons energy.
I_{om}	DC component of the maximum inductor current.
I_{pv}	Output current of the PV cell.
I_{sc}	Short-circuit current of the PV cell.
I_{sh}	Current in the shunt resistance of the PV cell.
K	Boltzmann's constant.
N_s	Number of cells in series.
P	Maximum power of the PV panel.
R_s	PV cell series resistance.
R_{sh}	PV cell shunt resistance.
V_{mp}	PV panel voltage at maximum power.
V_{oc}	Open-circuit voltage of the PV panel.
V_{pv}	Output voltage of the PV panel.

LIST OF ABBREVIATIONS

A/D	Analog to digital.
LPF	Low pass filter.
MPPT	Maximum power point tracking.
P and O	Perturb and observation.
PV	Photovoltaic.
P-I	Power-current characteristics of PV panels.
P-V	Power-voltage characteristics of PV panels.

CHAPTER 1

INTRODUCTION

1.1 Introduction

The population growth and energy use by humans are directly proportional. This direct proportionality increase the concern about the lack of Non-renewable energy resources. The oil reserves start decreasing day by day. This decreasing trends of oil reservoirs compels scientists to start thinking about alternative renewable energy resources. These renewable energy resources may not harm and pollute the environment. Moreover, this renewable energy must secure a decent life for the new coming generations. The renewable energy will diminish the great human concern about the energy crisis. Figure 1.1 and Figure 1.2 demonstrate the increasing nature of the renewable energies usage.

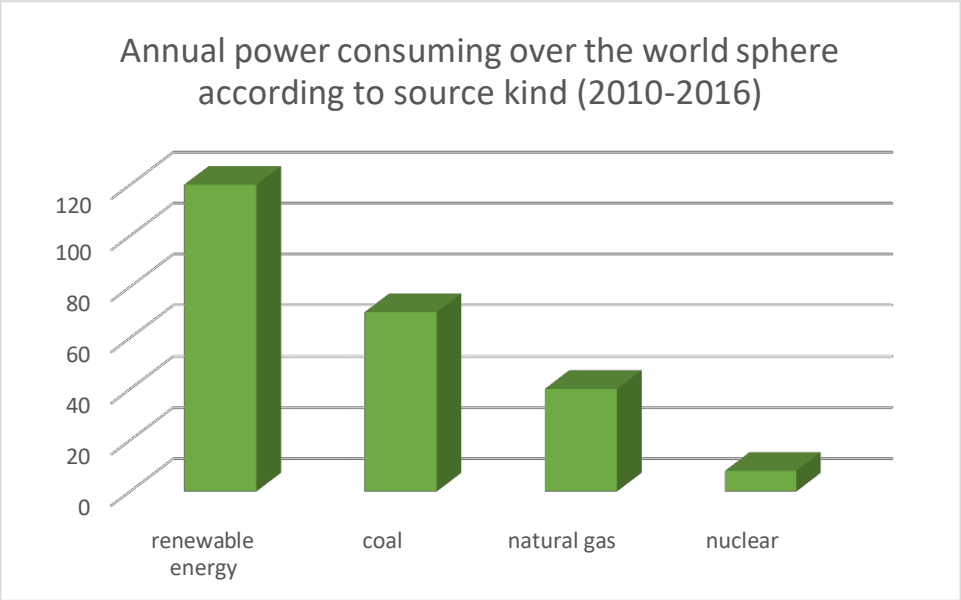

Figure 1.1 Annual power consuming over the world (2010-2016).

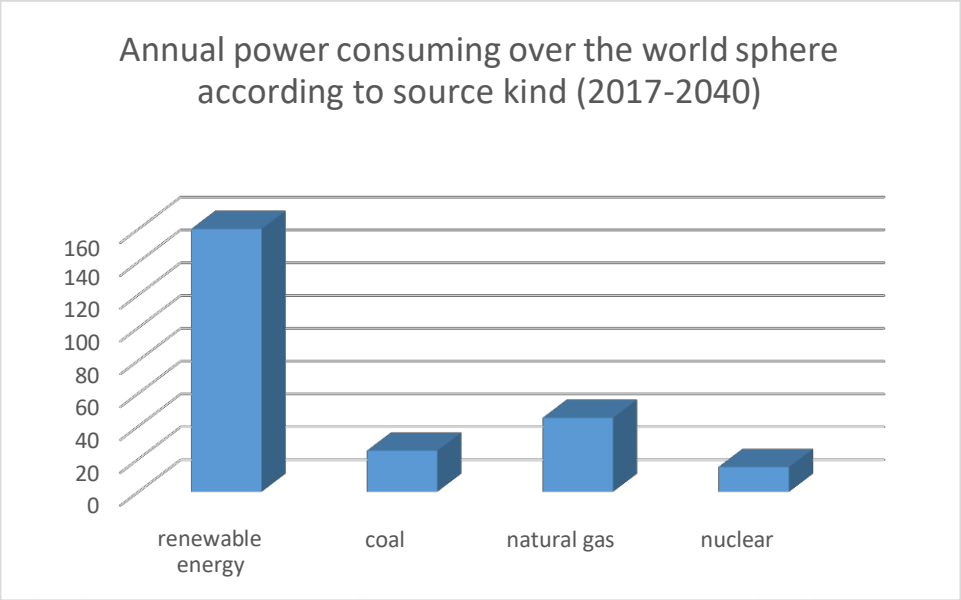

Figure 1.2 Annual power consuming over the world (2017-2040).

Due to energy entry into most areas of life, the human need for energy is increasing day by day. Additionally, the scarcity of petroleum energy resources (fossil fuels such as oil) results in international conflicts over them. Therefore, most countries have turned their attention to usage of renewable natural energy resources (biomass, geothermal, photovoltaic and wind) to produce energy in a continuous and reliable way. Figure 1.3 illustrates the global renewable energy capacity.

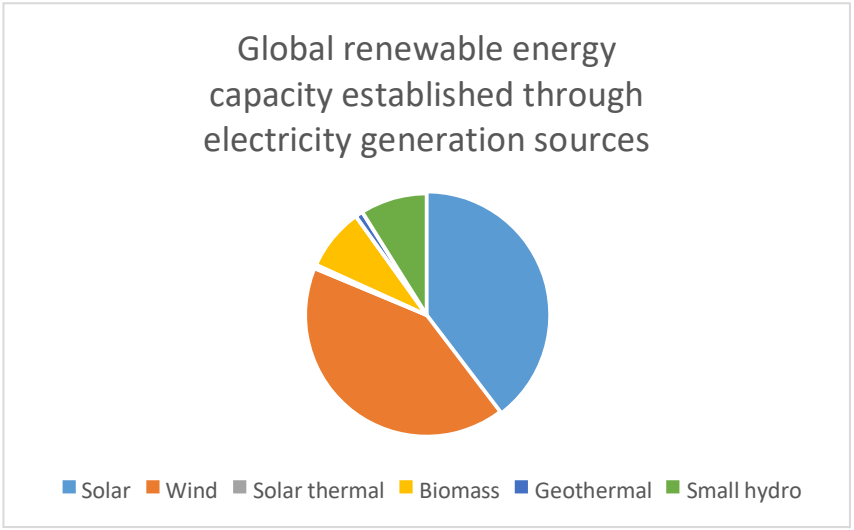

Figure 1.3 Global renewable energy capacity depends on electricity sources.

Solar energy systems have assured a great role and importance in ensuring alternative energy as a permanent future energy resource for most countries, particularly developed countries. The main reasons are the abundant availability of the sun in almost every spot of the earth, the remarkable development of solar system equipment and devices, ease of use, and high production efficiency. Despite of all these reasons, it suffers from some defects. The most prominent of which is finding and tracking the maximum power point. Many scientist and researchers have tried to overcome this defect [1-3].

The most important component of solar systems is solar cells that normally give (2-3) watts. This solar cell converts light energy into electrical energy. PV cells consist of semiconductor crystal materials that receive and absorb photons from the incident light and then release electrons, producing electrical energy. These solar panels are then connected in series to form a solar panel with high power for various applications.

1.2 Photovoltaic Systems Development History

Photovoltaic panels are composed of semiconductor materials that transform the solar radiation coming from the sun to its surface into electrical energy. The name Photovoltaic comes from the combination of the word "Phos" and "Voltaic". The word “Phos” means light in Greek and come from the unit of electric potential volt while the word "Voltaic" comes from the Italian physicist (Alessandro Volta) who invented the battery.

These systems have been in existence since many previous years and are in a state of exponential development. The first experiment was done 180 years ago. In 1839, the 19 years old Physicist Scientist Alexandre Edmond Becquerel, who discovered that the electrical conduction of two metallic poles in a conductive liquid increased with exposition to light. This discovery was a new beginning and revolutionized the world of Photovoltaic. In 1873, the sensitivity of selenium to light was noted by the Englishman Willoughby Smith. William Grylls and Richard Evans Day in 1876, found that electricity can be produce by exposing selenium to light [1]. Although these discoveries were unable to produce enough electricity to operate electrical equipment. However, they showed that solid materials can produce energy without the need for any warmth or kinetic mechanism.

In 1883, American inventor Charles Fritts founded the first Photovoltaic cell with 1% efficiency using selenium [2]. An entitled article "The Photovoltaic Effect" was published in 1905 by scientist Albert Einstein. In which, he explained in details the photo electric effect. Later on in 1921, due to this invention, he won Nobel Prize.
Similarly, the scientists Daryl Chapin, Calvin Fuller, and Gerald Pearson in 1954 at the Bell Telephone Laboratory in America invented the first 4% efficiency solar cell that could power electrical equipment. In 1960, these cells had been used in satellite systems. After the energy crisis of the 1970s, alternative energy sources related research attracts the attention of many researchers. In 1980s, photovoltaics were widely used in the electronic devices consumed in quotidian lifetime. Many calculators, clocks and radios were manufactured that were powered by batteries based on small solar cells at that time. Today, the usage of solar PV systems is growing about 25% every year.

1.3 PV Cell Characteristics

1.3.1 PV Cells Kinds

Photovoltaic panels can be divided into three generations when arranged chronologically. These are first generation, second generation, and third generation.

A) First Generation

The first generation includes both mono crystal and polycrystalline cells. The first generation is the cornerstone of photo electricity. To this day, it is one of the most preferred types of panels. When we check the installed electrical systems, we notice that the use of monocrystalline and polycrystalline panels has exceeded 95% [3].

Silicium is the second most abundant element after oxygen in nature. But it exists naturally in the form of silicon dioxide (SiO_2). In order to be used in the formation of photo electric panel, the purity of this material must be at least 99.99%. To achieve this, first both carbon and silicon dioxide are chemically react. Then the smelting process is applied with electric arcs of 2000 ° C. The oxygen atoms in silicon dioxide combine with carbon. It breaks down into carbon dioxide and carbon monoxide, and 99% of pure silicon. But this percentage of purity is not sufficient, so the silicon is introduced into the chemical equations to obtain the greatest possible purity then it is subjected to the distillation process. Finally, in the Siemens stage, the silicon is

introduced into reactors at high temperatures and decomposes to obtain multiple crystals of purity of 99.999%.

Monocrystalline PV Cells: These cells are obtained by two crystal formation methods called "Czochralski's contraction" and the "floating region" method of pure silicon [4]. The methods have been discovered by Polish chemist (Jan Czochralski) to produce high- purity silicon. First, pure silicium is smelted and liquefied. Then a rotatable crystal wand is slowly dipped into the silicone crucible and the silicone is expected to solidify on the wand. After this operation, the silicon, which appeared to harden, is withdrawn with precise and clear methods very slowly. As a result, high-purity silicon becomes a cylindrical ingot. The difficult part in making mono crystal comes after this stage, cutting these cylindrical ingots into washers is a very difficult process. After the cutting process, layers appear, which are called chips. These chips are the main component of solar cells. Then, the cells used in the panels are produced by combining the metallic dispensing rods and steroids, respectively. When these cells come together, the solar panel is ready. Therefore, monocrystalline panels are produced with maximum purity and thus have high efficiency.

According to a report by the Honorable Institute in 2018, the efficiency of monocrystalline has reached 26.7% in a laboratory environment so far, while the efficiency of the products used in the market is 19% -21% [5]. Due to the high purity, it has a dark color and a homogeneous appearance. With these properties, it can absorb a large amount of light, so that it can work efficiently also in places with low light. Because of its high efficiency, especially in places where there is no large area, it has got a great attraction in the market. However, due to its difficulty in production, it is of a very high cost, and Mono Crystal is considered one of the most expensive types of panels.

Polycrystalline PV Cells: The Czochralski method is an expensive and difficult one. Therefore, polycrystalline was manufactured to reduce the manufacturing cost. In the production of polycrystals, the process of forming the cylindrical ingot and the difficult cutting process used in the production of monocrystals is replaced by melting polysilicon directly into alloys. Then, the cutting process is performed. Therefore, it is not homogeneous and has a polycrystalline structure. Since the purity of the crystal structure decreases as the homogeneity is moved away. The level of efficiency is also

Lower than that of monocrystalline at the same rate. According to a report by the Honorable Institute (Photovoltaic) in 2018, the efficiency of polycrystalline has increased to 22.3% in a laboratory environment so far. The efficacy of the products used in the market today ranges between 16% and 19%. Polycrystalline is one of the most widely used panels in the market. The reason for this is the low cost and ease of manufacture as compare to Mono Crystal. However, polycrystalline is less heat tolerant than monocrystalline. It works less efficiently than Monocrystalline, this condition is considered a negative point in the life of the plate.

B) Second Generation

The second generation is the one that contains cells with thin membranes. It is formed by applying one or more thin layers over the coating material. These types of micrometer-thick cells have a large surface, because the materials used are very thin. It is a useful kind in terms of material quantity. Because of the reason, second generation material are very good for producing flexible, lightweight panels. Thus, this type of panels is easy to install in places where regular panels are difficult to install.

Due to the lower temperature treatments, it works more efficiently compared to monocrystals and polycrystals at higher temperatures. Therefore, the rate of corrosion is less compared to other types. The purpose of the thin film cells is to produce high-efficiency and low-cost units utilizing the advantages of minimal materials and an easy production line.

C) Third Generation

Efficiency and cost are among the most important factors influencing the solar chargers today. The thin cells present in the second generation contributed to the development of solar energy, but scientists continued to search for others methods to obtain greater efficiency, less time consuming, and having less cost. And for this reason, new types of cells were discovered, such as organic cells.

1.3.2 Functioning Principles of PV Cell

The fundamental compound of PV panels is solar cell, which is made of primarily silicon and other materials as well. In order to understand the functioning of photo electrics, we need to understand the functioning of semiconductor materials. As solar cells have semiconductors materials that have capability to produce electrical

current when exposed to electromagnetic rays. The fallen radiation detached the electrons from the atom. As a result an electrical current is produce [6-7]. A P-N junction which is consist of two various coat of silicon represent the main part in solar cell. In N-type, the atoms with one more parity electron is titled granter while in P-type, it is titled as receiver. Once the two coat meet with each other near the surface of the solar cell, free electrons travel from the N-type to the P-type, leaving a positively charged hole through the granter. Conversely, free holes in P-type move into N-type, leaving behind a negatively charged region in the receiver. This produces an electrical range through the two coats. This electric field drags electrons and holes in reverse orientations therefore the current can stream in only one orient. Electrons can travel from the P-type to the N-type and holes travel in the reverse order. Figure 1.4 demonstrates the generation of an electric field due to electrons and holes movement in a P-N junction material.

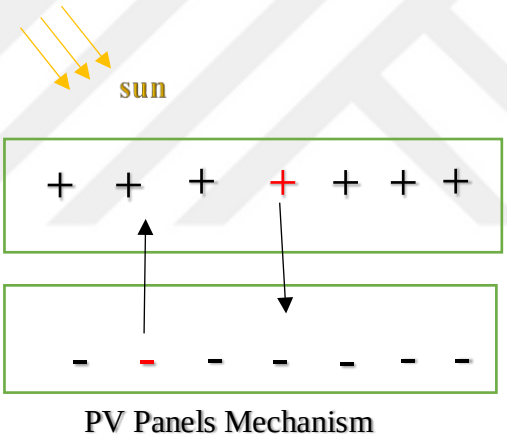

Figure 1.4 Working mechanism of P-N junction.

Both sides have metallic connections that gatherer electrons and holes and allow current to flow. The radiations directly fall on N-type. Sundry metal are used as a connection in this junction. Solar cell construction has been clarified. The cell function starts when the photons fall on the solar cell. Three various situation can occur, a few photons are mirrored from cell's roof and do not get through cells, another photons are not reflected from cell's surface and low-energy photons often remain over the cell without any effect. To be able to create a binary electron hole, the energy level of the photons must be higher than the gap of the silicon belt. The charges (the electrons on the P-layer, the holes on the N-layer) move in the P-N junction in the obverse trend in an electric field. That creates a current in the cell, which is gathered via the metal

connections on two parts as shown in Figure 1.4. The current generated is directly proportional to the rays. Greater intensity of fallen radiation means it has more photons and sufficient power to make additional electron-hole couple, therefore higher current in solar cell will be generated.

1.3.3 The Model of PV

The photovoltaic consists of an N-P junction made of thin semiconductor strips (layers), which has electrical properties slightly different from the diode represented by Shockley's equation. Figure 1.5 illustrates, the simplest equivalent circuit of a solar cell, consist of a source of current [8]. The output of the source current $I_{pv.cell}$ is directly proportional to the incident light on the cell. Therefore, the modeling process can be developed according to the following equations [8].

$$I = I_{pv,ell} - I_d = I_g - I_s * [e^{\frac{q*v}{a*k*t}} - 1] \quad (1.1)$$

where,

I_g: The current generated by the incident light.

I : Diode Schottky equation.

I_s: Diode leakage current.

q: Electron charge $1.602*10^{-19}$.

k: Boltzmann's constant $1.3806503*10^{-23}$.

T: Conductor temperature (kelvin).

α: An ideal diode ranges from 1-2 for mono silicon cells.

The basic Equation (1.1) of a PV cell does not represent the *V-I* properties of the working model. Since the business model consists of delivering multiple cells PV. Therefore, additional parameters such as R_s, R_{sh} must be included [9].

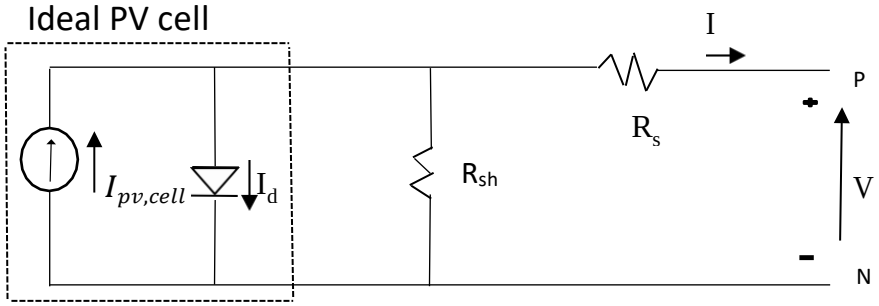

Figure 1.5 The ideal circuit for a photoelectric cell.

$$I = I_{pv} - I_0 * [e^{\frac{(V+R_s*I)}{V_t*a}} - 1] - (V + R*I)/R_{sh} \quad (1.2)$$

where,

V_t : It is the thermal voltage. Mathematically can be represented as follows [9].

$$V_t = \mathrm{k} * {}^{T}/_{q} \quad (1.3)$$

k: Boltzmann's constant $1.3806503*10^{-23}$.

q: Electron charge (coulomb).

T: Conductor temperature (kelvin).

The light generates a stream from the array of cells, linearly depends on solar radiation. It is also affected by temperature according to the following equation [9].

$$I_{Pv} \equiv (I_{Pv,\mathrm{n}} + K_i * \Delta T) * G/G_n \quad (1.4)$$

where,

$I_{Pv,\mathrm{n}}$: Current generated under exponential conditions.

$\Delta T = T\text{-}T_n$: Real and standard temperatures, respectively.

K_i: The temperature coefficient of the current.

G: Solar radiation W/m^2.

G_n: Solar radiation at standard conditions $1000W/m^2$.

The saturation current of the diode I_0 depends on the temperature. As shown in the following relationship [9].

$$I_0 = I_{0,n} \ (T/T)3 * e^{\frac{(q*E_g)}{(a*k)} - (\frac{1}{T_n} - \frac{1}{T})} \quad (1.5)$$

where,

E_g: The energy gap of a semiconductor, which is the energy field in a solid body in which electrons cannot exist.

$I_{0,n}$: The nominal saturation current, mathematically can be written as [9]:

$$I_{0,n} = \frac{I_{sc,n}}{\frac{V_{oc,n}}{e^{v_{t,n}*a} - 1}} \quad (1.6)$$

From the previous two equations, we find that,

$$I_0 = (I_{sc,n} + k_i * \Delta T) / (e^{\frac{(V_{oc,n} + K_v \Delta t)}{v_t * a}} - 1) \quad (1.7)$$

where,

$V_{oc,n}$: Open circuit voltage is exponential.

$I_{sc,n}$: The nominal short circuit current.

V_t: Thermal voltage.

K_v: Thermal coefficient at voltage $V_{oc.}$

$$V_t = N * k * {}^{T}/_{q} \quad (1.8)$$

Equation (1.8) expresses the thermal potential of the model with number of the cells (N_s) connected in series. The cells are connected in series to generate huge amount of current and output voltage [8].

If the unit consists of N_p as a sub-link of a photovoltaic cell, then both the saturation current and the resulting photoelectric current are determined as follows:

$$I_{pv} = I_{pv,cell} * N_p \quad (1.9)$$

$$I_0 = I_{0,cell} * N_p \quad (1.10)$$

In Equation (1.2) the value of the serial resistance R_S and the parallel resistance R_{sh} of a module are unknown. Therefore, these values must be found. And Equation (1.2) is mathematically derived from Figure 1.6, which is basically a relation between (I-V). From this Figure 1.6, provides three clear points [9].

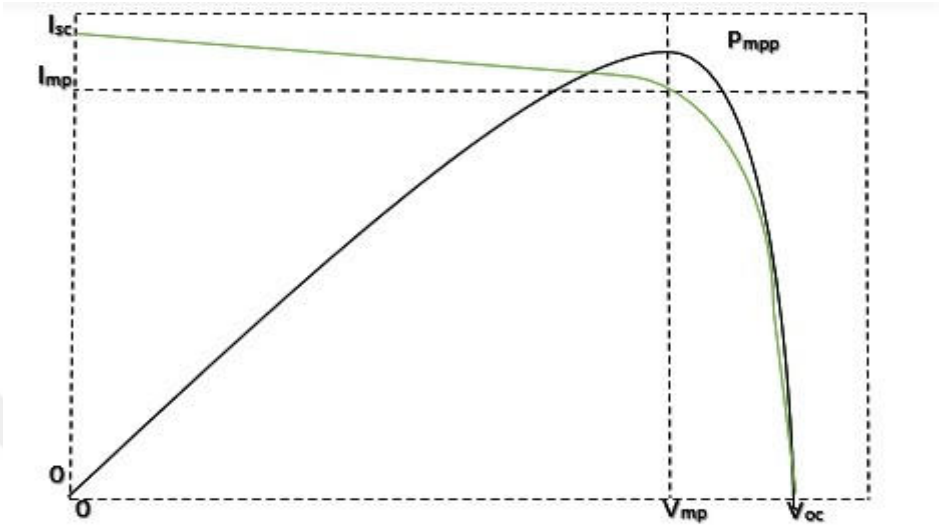

Figure 1.6 Photovolatic I-V characteristics plot.

I) The open circuit coordinates are determined by variables (v_{oc}, *0*).

II) The coordinates of the shorted circuit are determined by the variables (*0*, I_{sc}).

III) The coordinates of the maximum power point are determined by the variables (V_{mp}, I_{mp}).

I) Open circuit: This condition occurs when the load is separated from the module. In this case, the voltage is called the open circuit voltage (V_{oc}). Mathematically open circuit voltage can be computed as follows:

$$V_{oc} = \frac{a * k * T_{cell}}{q} * \ln \frac{I_{pv}}{I_0} \quad (1.11)$$

II) Short Circuit: In this case, the connected load on the module is having zero resistance. When a current called short circuit current passes (I_{sc}) and the voltage on both ends of the model is zero, the circuit is called short circuit. The short circuit current can be mathematically calculated as follows:

$$I_s = I_{pv} = K * G \quad (1.12)$$

where *K* is a constant.

III) Maximum power point: At maximum power point, we gain the maximum voltage (V_{mp}) according to voltage (V_{oc}). Mathematically, maximum voltage can be computed as follows:

$$V_{mp} \approx 0.8 * V_{oc} \tag{1.13}$$

(I_{mp}) is related to the current (I_{sc}) in the following form.

$$I_m \approx 0.9 * I_{sc} \tag{1.14}$$

The standard operating conditions are the best operating conditions that represent solar radiation equal to (1000 W /m^2), cell temperature equal to 25°C and spectrum distribution (*AM*) equal to 1.5.

1.3.4 Features of Power

Both V_{pv} and I_{pv} are extremely important to obtain the maximum possible effectiveness of the PV modules and this is illustrated in figures (1.7) - (1.9). Under the regular conditions of a systemic PV cell, we will be able to look closely at the behavior of voltage as a function of current. The available voltage and current features (I-V) are illustrated in Figure 1.7. The voltage in this case is restricted by the open circuit. According to the *I-V* relationship both V_{oc} and current are determined according to the law of short circuit current I_{sc}. The amount of output energy for both V_{pv} and I_{pv} can be obtained by means of the formula $P_0 = V_{pv} x I_{pv}$.

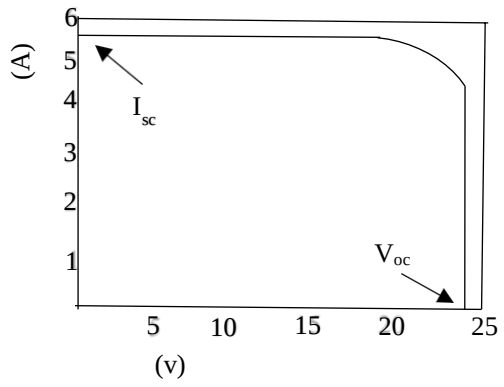

Figure 1.7 Features of power PV module.

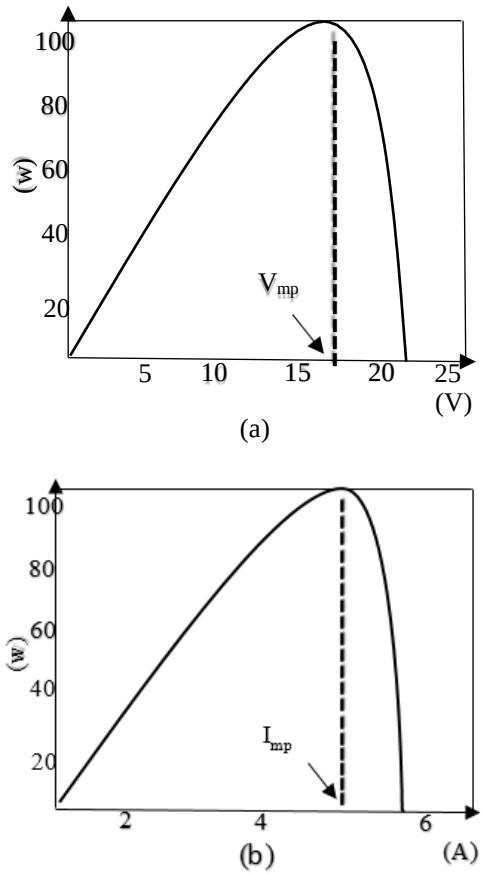

Figure 1.8 Features of Power PV module according to voltage and current.

1.4 Maximum Power Point Tacking (MPPT)

According to climatological changes, the *I-V* features of the PV panels also varies. From the variant nature of *I-V* curves, one can notice in the results that illustrate variant curves of the *I-V*, and this is because of the changes in the degrees of exposure to the sun. Figure 1.9 and Figure 1.10 illustrates sunlight and warmth influence of *I-V* features of the solar panels.

The maximum current I_m, is because of these alterations in the *I-V* features. Figure 1.11, illustrates the maximum current I_m. Similarly, Figure 1.12, illustrates the maximum voltage V_m. One can clearly notice that I_m is greatly influenced by the change of sunlight intensity, while the variable warmth greatly affects the V_m. Therefore, the *MPPT* notion is based on observing and trying to track and get the highest point I_m and V_m beneath these variable weather situations [10].

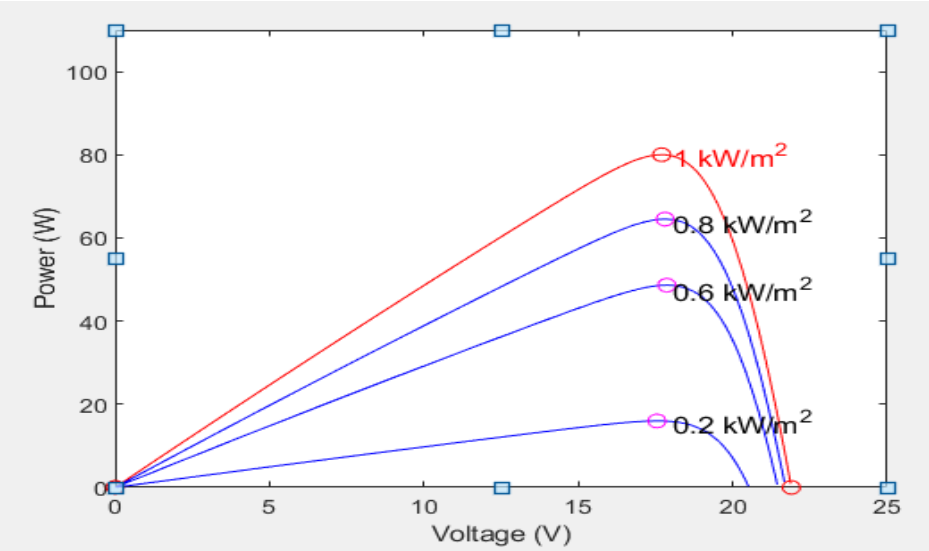

Figure 1.9 Sunlight influence of the I-V features of solar panels.

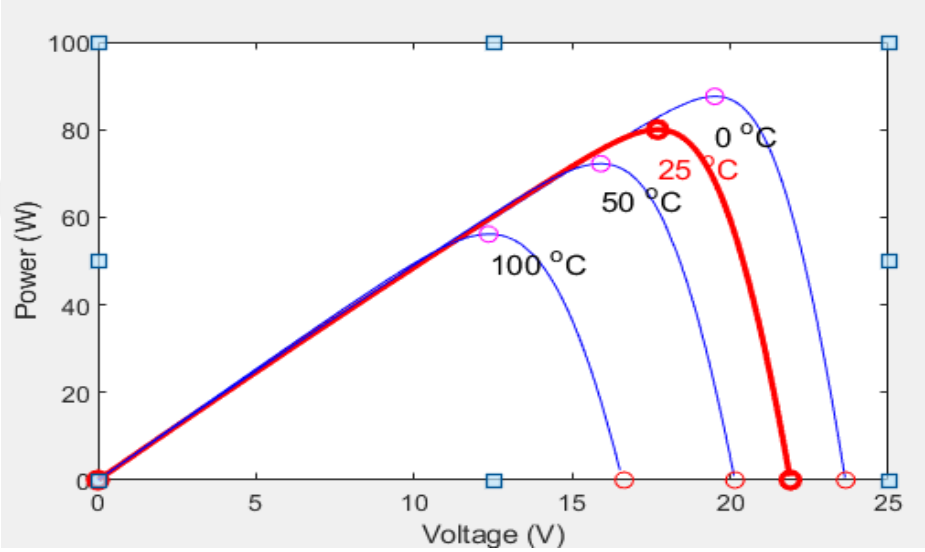

Figure 1.10 Warmth influence of the I-V features of the solar panels.

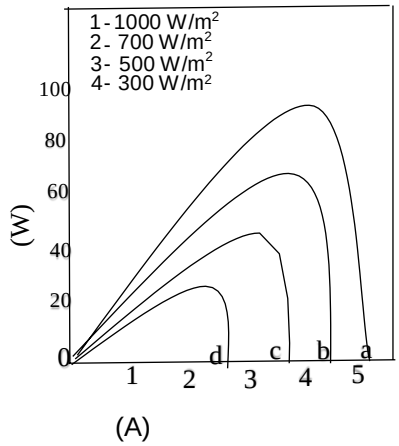

Figure 1.11 The change in P-I characteristics of the PV according to the sunlight.

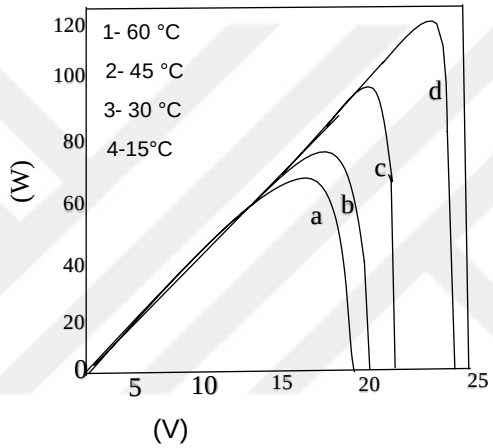

Figure 1.12 The change in P-V characteristics of the PV according to the warmth.

Figure 1.13, illustrates the basic diagram of solar panel, DC-DC converter and load [10-11]. The DC-DC converter varies the duty cycle periodically which results in a verified PV and load in order to catch the highest power. The main function of MPPT is changing PV to get the ideal point (I_m,V_m) under these changeable weather situations.

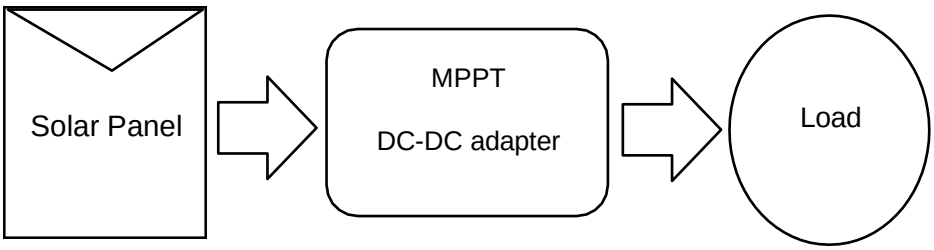

Figure 1.13 MPPT diagram.

1.4.1 Algorithms of MPPT

As discussed earlier, the main objective of MPPT modules is to convert the function point of the PV modules to the ideal point. This can be obtain by swapping the DC-DC parameters [11]. Figure 1.14, demonstrated the ideal control diagram of MPPT.

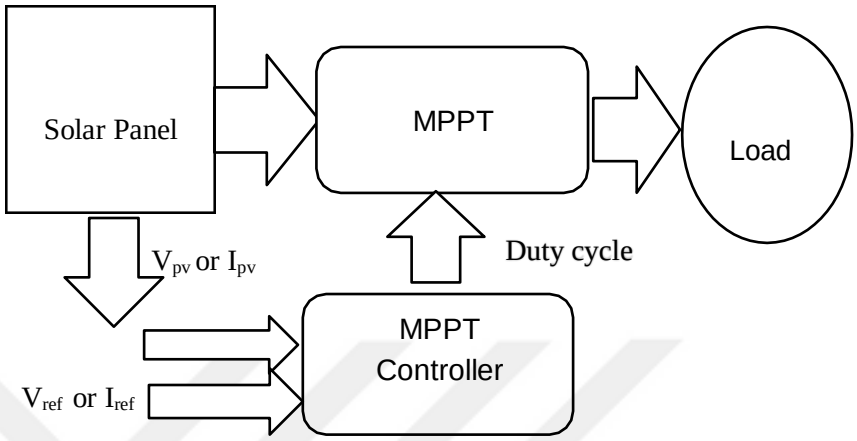

Figure 1.14 Ideal control diagram of MPPT.

Multiple MPPT rely on multiple ways to continuously enhance reference signal to obtain as close to the best ideal points (V_m, I_m). It can be said that there are two mode used by MPPT units to change the functioning of the PV.

1) Observe the Voltage Returns:

This method depends on modeling the optimum voltage V_{mp} and identifying it as a reference (V_r). Then they try to boost the value of the PV panel voltage V_{pv} to the reference voltage by making some changes in the transformer [11].

2) Observe the Current Returns:

This method depends on modeling the optimum current I_{mp} and identifying it as a reference (I_r). Then they try to boost the value of the PV panel voltage I_{mp} to the reference current by making some changes in the transformer [12].

Moreover, some of these methods use the duty period as a monitoring reference instead of voltage or current [13, 14]. The hill climbing mode and the incremental mode are the most used MPPT methods, which will be discussed further as follow.

Hill Climbing: This method relies on a trial and error approach. For example, the voltage is sampled at certain intervals, the resulting energy is studied to make sure that the energy slope was positive or negative. Otherwise, the sampling interval is must be changed [12, 13].

Incremental Conductance Mode: The method is based on the energy derivative associated with voltage (dP / dV). The derivative must be 0 at the highest energy level. This mode also refreshes the control reference according to the length of the output power side [26].

1.5 Report of Case

A lot of algorithms for MPPT were presented, but each of these algorithms has specific defects. Shakiness and change of energy in the stable situation are among the most common flaws in the algorithms. Moreover, one of the disadvantages of this type ofalgorithms is that it requires more time to take the required samples. Additionally, this type of algorithms is costly. Below, the most important parameters to get an ideal MPPT algorithm are discussed.

- Response dynamically: Known as the speed required to constantly following the highest power point. The more the value of the response dynamically, the more will be the resulting energy.

- Response Stability: It is known to reduce the energy waste when the function point comes to highest power point.

- Fast Alteration in Climate Status: In case of days, when the weather status is changing repeatedly and quickly, the algorithm can have volatile results which lead to incorrect functioning of MPP.

- Easy to Usage: It is crucial in algorithms because it is one of the most important factors in getting the required samples faster.

1.6 Purpose of Study

In order to get rid of the mentioned defects, this research work presents a new advanced MPPT algorithm that is simple and strong. The main objective of the research work is to make the algorithm accurate and suitable to be operated on STM microcontrollers.

The designed algorithm must be an efficient, and economic to obtain maximum photoelectric energy. In addition, the idea can be commercialize and more benefits can be gained practically. The main goals of the thesis are presented point-wise as follows:

1. The proposed algorithm is very easy to implement and cost-effective. In addition, the proposed algorithm is based on the properties of the DC-DC boost converter and STM microcontrollers.
2. The proposed algorithm must include developed solutions, which is updated based on the reference changes. In addition to this, the new algorithm will be able to beat problems of variable climate conditions to obtain more accurate results.
3. The designed algorithm should be tested on the simulation computer program and the result must be compared with the results of an ideal or normal MPPT. This way, one will be able to check the response speed and accuracy to verify the output enhancement.
4. A prototype for the devices based on the booster and micro-controller (STM) has been designed, by design PCB to check the real results as well.

1.7 Outline

1. From second chapter onwards, a detailed explanation of the basic meanings used in MPPT algorithm is presented. Moreover, the appropriateness of the chosen studies is also demonstrated.
2. The third chapter presents the specific conditions and modes required for enhancing the output in volatile ambient status.
3. The PCB design and experimental implementation is presented in chapter 4. Additionally, the experimental and simulation analysis of the proposed algorithm are also presented in chapter 4.
4. The fifth chapter discusses the findings and future aspects of the project.

CHAPTER 2

LITERATURE SURVEY

2.1 Introduction

This chapter explains the MPPT algorithm. The Perturb and Observation (*P & O*) method, and the open circuit method will be clarified. Some other concepts will be also clarified. The designed MPPT algorithm will be discussed and explained with more details. All current developments in this area will be reviewed as well.

2.2 Theory of MPPT

2.2.1 Perturb & Observation (P & O) Algorithm

This technique is also known as hill climbing approach. The main objective of this method is to reach or obtain the ideal point. The variable or changeable reference is analyzed and updated by trial and error method to catch the nearest point of MPP [10-11]. The flow diagram of the *P & O* algorithm is illustrated in Figure 2.1. The algorithm continuously changes the step size *r[n]* according to the direction of power slope. The power is increasing continuously till reach the MPP, where the variable reference is r[n]. The variable $P_0[n]$ illustrates the output power, $V_p[n]$ shows the output voltage of the PV and $I_p[n]$ represents the outcome current. The power $P_0[n]$ is compared with the one calculated previous $P_0\ [n-1]$. If the result is $P_0\ [n] < P_0\ [n-1]$, then the turbulent path of the reference variable changes in the opposite direction. The method used is very simple and easily accessible and does not have complex computation. However, this method continues to distort the reference even when it reaches a steady state. Therefore, apparently produces constant fluctuations in the generated energy.

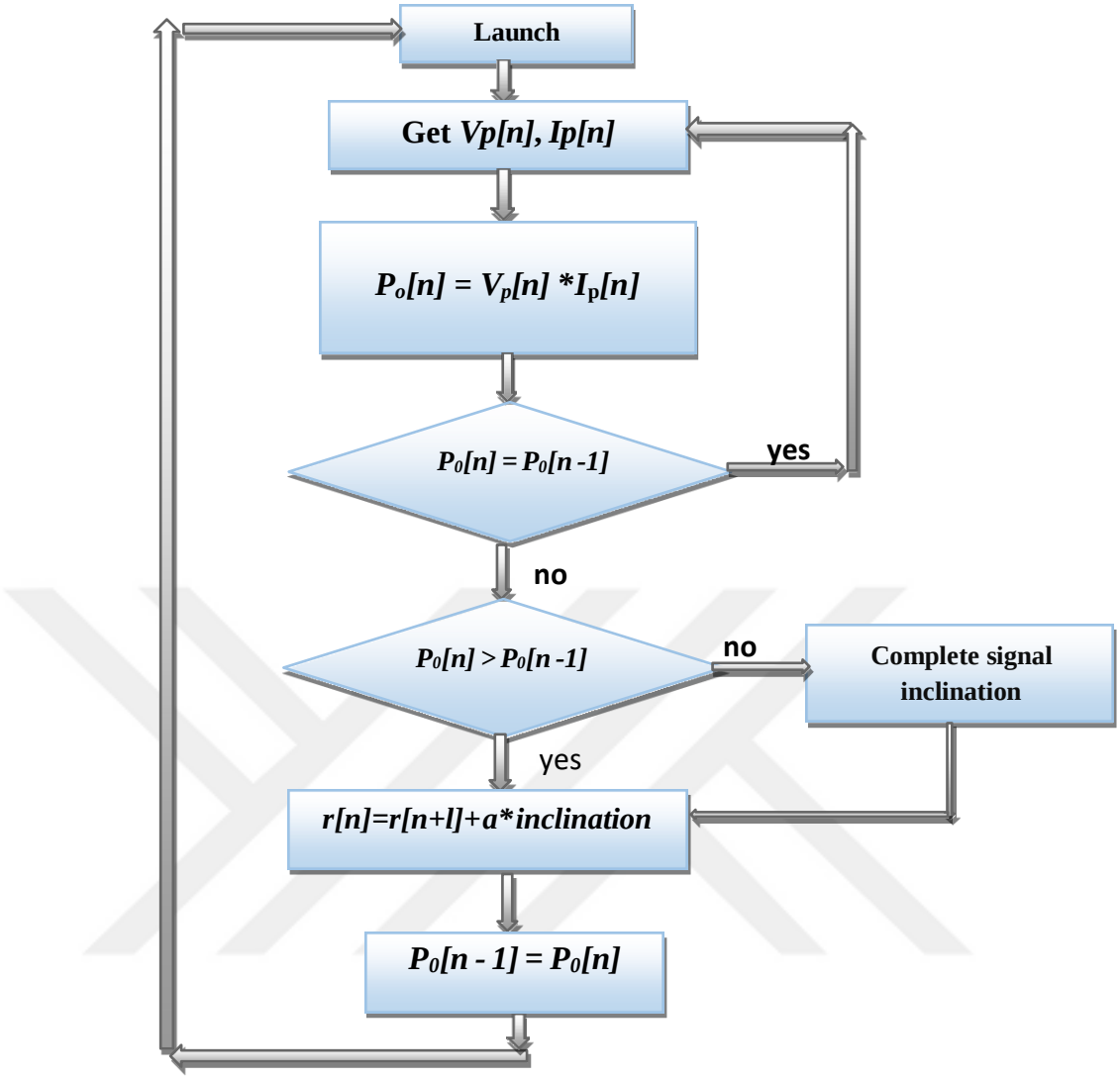

Figure 2.1 P & O algorithm diagram.

2.2.2 Open Circuit Mode

The constant voltage mode or open circuit mode mainly depends on that 76% of the open circuit voltage (V_{oc}) that constitutes of the maximum voltage of the V_{mp} power. Finally, the MPPT is disconnected at specific times and $0.76 * V_{oc}$ is set as a reference to get the value of open circuit voltage of the PV [15]. Short circuit current mode is also called constant current mode and it is giving a constant voltage. This mode mainly depends on that 90% of the short circuit current I_{sc} that constitutes the maximum volume of the power current. Additionally, the $0.9 * I_{sc}$ has been set as reference.

The MPPT is disconnected from the PV module at specific times to get the value of short circuit current. This mode is one of the simplest because it involves a single

multiplication to set the reference *V* or *I*. But, on the other hand the big disadvantage of this method is energy loss due to MPPT is disconnectivity from the PV module at specific times regardless of the complexity of the devices.

2.2.3 Alternative Techniques

Other major algorithms of MPPT can be expressed by the capacitance of parasitic mode, and this mode can be achieved through ICM. This algorithm has the advantage of neutralizing the reference variable of the sequence taking into account the average fluctuation of the unit's voltage. Some researcher also worked on nonlinear property of PV modules by using nonlinear techniques like fuzzy logic [16-24] and neural network techniques [17-25]. But these algorithms require complex mathematical operations in addition to the adaptive inability required when developing a PV system.

2.3 Implementation and Optimization

2.3.1 Improved MPPT with Microcontroller

The authors in [11], designed a comprehensive and understandable algorithm on MPPT for monitoring systems. Perturb and Observation (*P and O*) and specific inspection changeable duty cycle to fully activate the MPPT system are utilized in designing the algorithm. The transformer's duty cycle is kept monitoring via using pulse wave modulation (*PWM*) module. The values of *V, I* of PV panel are obtained through analogue to digital converter (*A/D*) converter for reading voltage and current. The controller is set to check the panel's voltage and current values through the former sampling at specific time to compute *P[n]* and *P[n-1]*.

Comparison is done between the values of *P[n]* and *P[n-1]*. Finally, the direction of turbulence path of the duty cycle is changed by the *PWM* according to results of *P[n] < P[n-1]*.

2.3.2 Adjusted Hill Climbing

The research works in [18], provide an idea to improve the changeable reference used in Hill Climb method. The difference in the forces produce the sample ($a[n] = F * \Delta P$, where F as constant). The adaptable step size $a[n]$ is periodically developed in accordance with the difference in the forces. As a result, when the step size is large,

the instantaneous point goes further away from the ideal point and when it is a small step the instantaneous point goes close to the ideal point. This algorithm contains an online order of the various parameters of the hill climb process as well. This method provides a state of dynamic velocity and the possibility of reaching a stable state.

2.3.3 Developed Perturb and Observation (*P & O*)

The authors in [15], investigate the reasons for chosen of the algorithm parameters *P* and *O*. As per specific MPPT systems, the parameter characteristics (*P and O*) are based on DC-DC converters. In the studied system, the voltage is used to enhance the response of *P* and *O*. We can take the boost converter as an example. After performing the assignment process for the parameters, the last results of the simulation computer program make the system effective.

2.3.4 Smart MPPT via Controlling the Top Current

An innovative algorithm from Perturb and Observation is enhanced [12]. That algorithm takes the characteristics of *P* and *O* in terms of plainness and quickness, then performs the optimization process by using fuzzy logic control. Moreover, an idea of top current is adopted, and this idea is applied to find the instantaneous amount of the current instead of the mean amount of the current. Hence, according to the modification of *I, V* of the PV, the current signal reference is checked and updated continuously. After this, the simulation computer program results of the algorithm are shown under variable weather situations, the interim improvements and fixed solutions are revealed.

2.3.5 MPPT while Checking the Climate Status

The researcher tried to find new parameters i.e., the effect of changing climate conditions, that may affect the performance of PV panels. This algorithm is based on the linear characteristics between highest power (P_M) and highest power current (I_{MP}) under variable weather situations. Depending on this step, a foreteller stripe is configured to follow the highest power point. Thus, the function point is chosen according to the foretelling line and in this way, the orientation of the signal changing is specified. The output response demonstrates a clear enhancement.

2.3.6 Fuzzy Logic Systems

The fuzzy series theorem was designed to solve real world problems. Fuzzy can successfully symbolize human knowledge of complicated problems. Fuzzy group theories and fuzzy logic can play a statutory role to mathematical present and enhance the problems. Fuzzy logic base system takes the climate conditions as an inputs. The fuzzy logic systems gives output according to the designed fuzzy mechanism. In the literature, terms such as fuzzy system, fuzzy model, fuzzy rule-based system, fuzzy observation unit, or fog associative recollection are exercised interchangeably relying on the kind of enforcement. Its major features include the symbolical exemplification of information in the form of indefinite (if, then) subjunctive rules.

2.3.7 Neural Networks System

A neural network is a series of algorithms that endeavors to recognize underlying relationships in a set of data through a process that mimics the way of human brain operation. In this sense, neural networks refer to the systems of neurons, either organic or artificial in nature. Neural networks can produce the output according to the changing input; so the network generates the best possible result without needing to redesign the output criteria. The concept of neural networks, which has its roots in artificial intelligence, is swiftly gaining popularity in the development of system to solve real world problems.

CHAPTER 3

PROPOSED ALGORITHM FOR MPPT

3.1 Preface

The speed and constancy of MPP have been enhanced in the proposed *P* and *O* algorithm. The problem of weather variations and their impact on the performance of the solar panel has also been controlled and addressed. Despite the algorithm's simplicity, it is preferred to use a developed STM microcontroller in the proposed algorithm. The STM microcontroller can add many advantages to the electronic circuit, as well as its increase the possibility of using the circuit in the commercial market. Moreover, it has not expensive and have reasonable cost. The hardware specification requirements are simple. The proposed algorithm select the duty cycle as reference. Modern method has been based on the updated version of MPPT. This may use different types of duty cycle method. Moreover, the proposed MPPT algorithm can develop and adjust more accurate and efficient results (by improving its performance). DC-DC boost circuit is applied as power alternator and step up circuit. Therefore, certain features of the boost circuit can affect the designed equations directly.

3.2 Properties of Proposed Algorithm

As we mentioned previously that the normal P and O algorithm (fixed step size) is not proper to adapt the nonlinear electrical characteristics of PV panel, and suffers of power losses.

In the proposed P and O algorithm, the efficiency of perturb and observe (P and O) maximum power point tracker (MPPT) has been enhanced. The efficiency improving has been achieved by ameliorating the tracking speed (transient response) and decreasing the steady state oscillation. A two step-size perturbation is utilized to decrease the oscillation and minimize the reaching time of operating point to MPPT. When the operating point is far from the MPPT, the perturbation is made larger to

ensure that the tracking speed is maximized. But as the operating point gets closer to the MPPT, the perturbation reduces.

3.2.1 Step Size

The most crucial parameter in MPPT system is step size selection. As it has a huge impact at whole algorithm. This impact has been demonstrated in Figure 3.1, the bigger step size, the more the response speed (higher following and reaching MPP). But this results in big energy fluctuations at stable state. On other hand, the lower step size will produce slower response speed (slower following and reaching MPP). But this results in low energy swings at stable state. As a result, the step size selection criteria depends on: the optimum balance between the temporary response rate and the stable state fluctuation, as manifested in Figure 3.2. The authors in [14], tried to get rid of step size selection troubles.

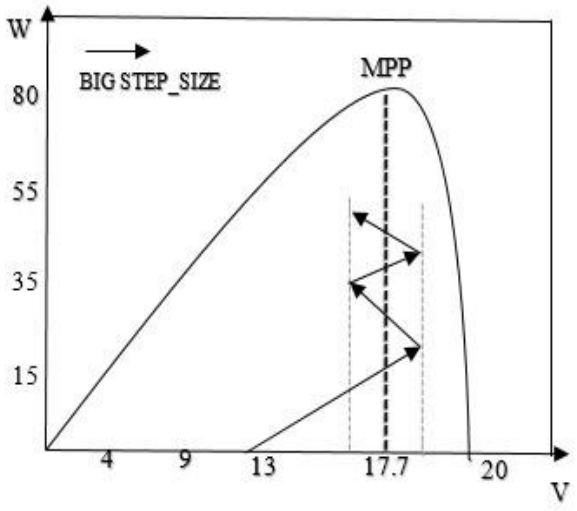

Figure 3.1 Big step size of MPPT.

Depending on the working point, the step size rate is selected and adjusted accordingly. Therefore, once the working point is very away from the MPP, the big step size rate is applied and once the working point is very near to the MPP, the low step size rate is applied. Consequently, it provides a quick respond as well as small energy fluctuations in a steady situation. Figure 3.3 shows the step size precept. Nevertheless, the place of a working point is needed and very important in step size precept (the placement relative to MPP) to rate the new step value.

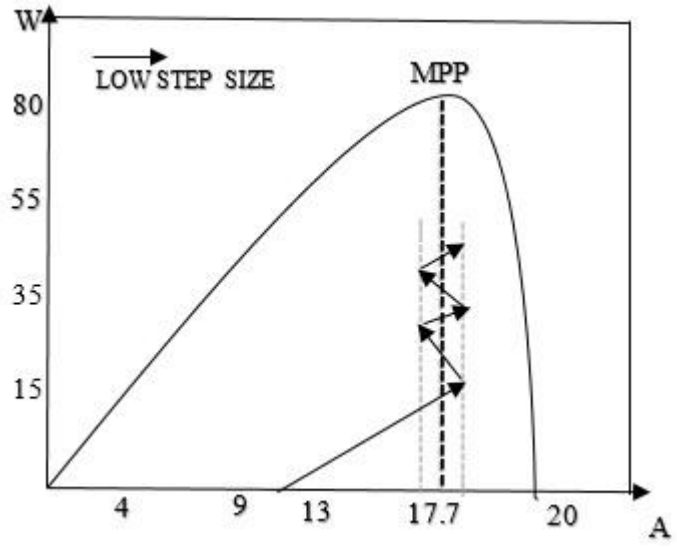

Figure 3.2 Low step size of MPPT.

While the previous studies like the one in [14], adapted step size principle to design MPPT algorithm. The algorithm takes first derivative power as relative to first derivative voltage in order to specify the placement of working point then adjust and verify the next step. Further detailed explanation about the first derivative power relative to first derivative voltage (V_p of panel) shown in Figure 3.4. When MPP reached whether left side or right side the value of first derivative power as relative to first derivative voltage (in absolute value) becomes zero at MPP.

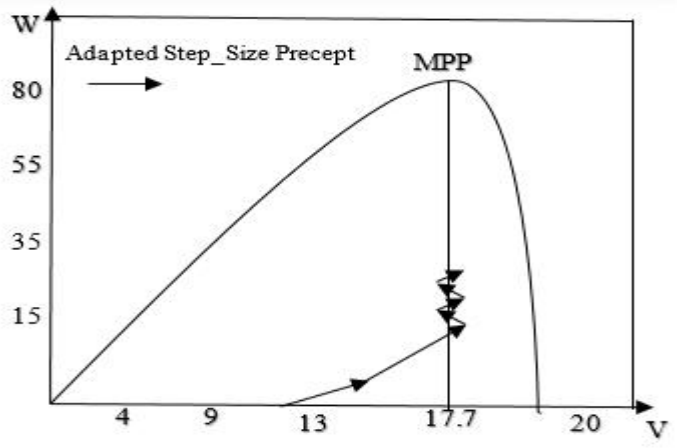

Figure 3.3 Adapted step size precept of MPPT.

Therefore, the placement of working point was specified using the value of first derivative power as relative to first derivative voltage (according to MPP). So as an outcome, changeable step size represents the reference.

$$S\,(n) = S\,(n\text{-}1) \pm V(n) \tag{3.1}$$

According to Equation (3.1), *S(n)* represents the new reference value, while *S(n-l)* and *V (n)* represents the current rate and the changeable step size, respectively.

$$\mathrm{V}(n) = K_N \left|\frac{dp}{dv}\right| \tag{3.2}$$

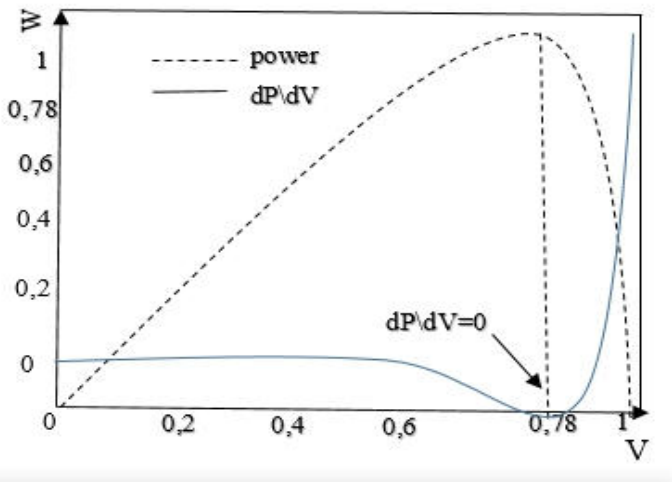

Figure 3.4 P-V Curve of solar panel with reference to dP/dV curve.

When the system update the step size, and working point meet MPP, the *V(n)* rate start reducing. For example, the value of first derivative power as relative to first derivative voltage becomes zero at MPP. One can see from Figure 3.4, that the left side of MPP (current zone) is plane while the right side of MPP change sharply (voltage zone) [27]. Subsequently, specifying step in left side of MPP is strict somehow (in current zone), unless working point of the panel lies near the boundary of the maximum achievable point. Significant differences in the value of first derivative power as relative to first derivative voltage at the right side of MPP(voltage zone) complicate the configuration of climbing agent K_n, that gives ability to fit the irradiation grades or improve the PV system (as increasing the PV module)[27].

A modified method to update the system is given in the proposed algorithm, the method depends on divide up the MPPT algorithm response into three regions (*I, II,*

III); where region *I* represents the first region and D_1 is used as big duty cycle to reach the MPP as quick as possible, therefore it gets a better transient response. The region *II* represents the second region and D_2 is used as very small duty cycle to avoid the fluctuations and decrease the power oscillations in the steady-state. Similarly, region *III* represents the third region and we used D_1 also to faster tracking of *MPP*. Figure 3.5 demonstrates the response MPPT in the three regions.

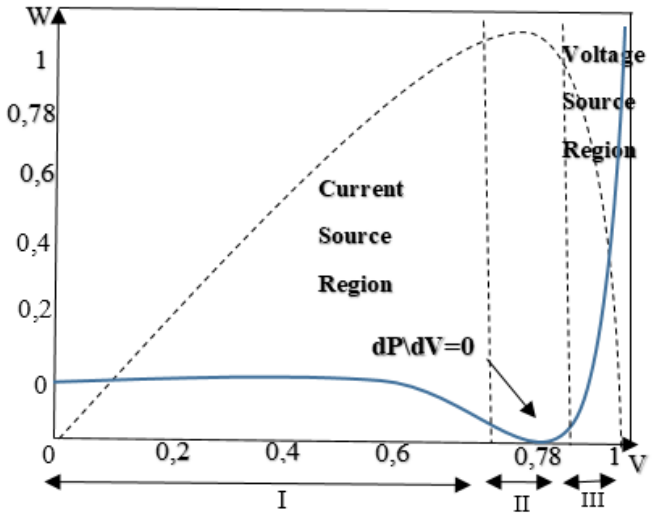

Figure 3.5 Designed algorithm response of MPPT system.

The power (*P*) is computed using the measured values of the voltage (*V*) and current (*I*) of the PV panel in the designed algorithm. The algorithm provides a perturbation (ΔD) in *D*, based on the change of *P* by the following rule:

$$D_{new} = D_{old} + \Delta D * slope \quad if \ P > P_{old} \tag{3.3}$$

$$D_{new} = D_{old} - \Delta D * slope \quad if \ P < P_{old}$$

In Equation (3.3), the slope indicates the direction of the perturbation, i.e. to the right (climbing) or to the left (descending).

Table 3.1 Determination of the slope value.

Sign of ΔP	Sign of ΔV	Slope value
Positive	Positive	+1
Positive	Negative	-1
Negative	Positive	-1
Negative	Negative	+1

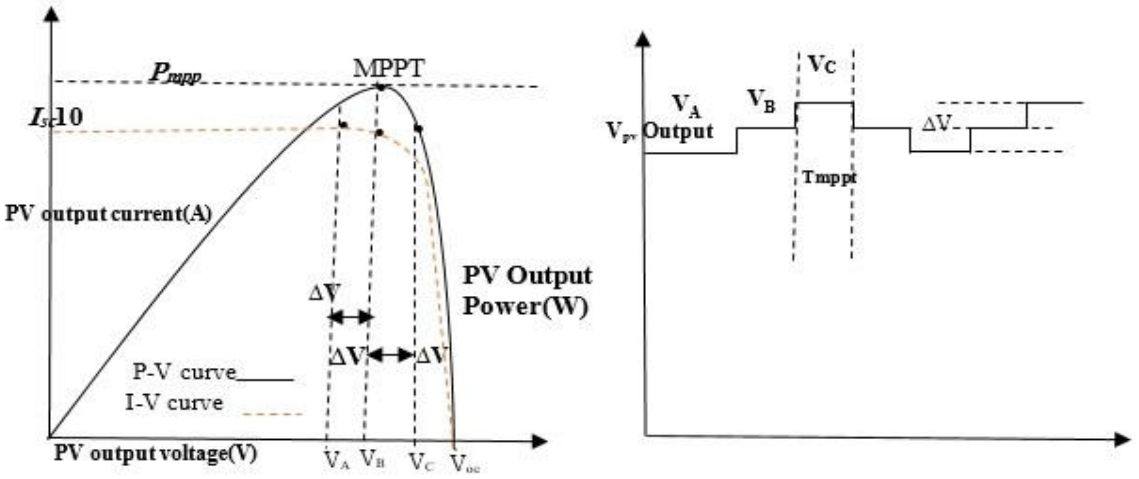

(a) I-V and P-V characteristics. (b) Perturbation step ΔV.

Figure 3.6 (a) I-V and P-V characteristics curve (b) Perturbation step ΔV.

Clearly, the size of the perturbation, Δ*D* is crucial; therefore, we supposed two values for duty cycle (D_1 and D_2) and separated the response of MPP into three regions to accomplish faster tracking MPP and better steady-state near the MPP.

If Δ*D* is large, the convergence is fast, but it results in large fluctuation in *P*, and vice versa. Whatever the case, the algorithm will push operating point to continuously oscillate around the MPP, as depicted in Figure 3.6. The loss is more if the perturbation size is large. The oscillation is highly undesirable as it results in significant energy loss [15].

The designed *P* and *O* algorithms can be based on the voltage or duty cycle. The mechanism intelligently varies the perturbation size (according to its region) to minimize steady-state oscillation. If the working point is away of MPP, the perturbation is made larger. This is to ensure that the tracking speed is maximized. As the working point gets closer to the MPP, the perturbation size is reduced until it becomes very small. Dividing the whole working scope into three various zones as demonstrated in Figure 3.5. The sorting zones are mathematically summarized in Equation (3.4), where $D_1 = 125e-6$, and $D_2 = 5 * 125e-6$. Based on the new method, the designed method's equations that specify the reference is shown below:

$$\mathrm{D}(n) = \begin{cases} \mathrm{D}(n-1) + D_1 & Region\ I \\ \mathrm{D}(n-1) + D_2 & Region\ II \\ \mathrm{D}(n-1) + D_1 & Region\ III \end{cases} \tag{3.4}$$

3.2.2 Proposed Algorithm Flowchart

A Comprehensive flowchart of the proposed algorithm is demonstrated in Figure 3.7. Initially the suggested algorithm launches via initializing the rate of voltage (*V*), current (*I*) and duty cycle (P_v*[*n*]* and *D[n-l]*). Besides, *D[k]* which is the initial rate of duty cycle has been set. Afterward, the proposed algorithm circle begins via capturing the voltage $V_p[n]$ and current $I_p[n]$ of solar panel which permits the algorithm to determine the produced power of solar panel via $P_o[n] = V_p[n] * I_p[n]$. Therewith, the major factors of designed MPPT algorithm *(*$\Delta P[n]$ and $\Delta V[n]$*)* are computed. After learning those important factors, the current working point region is determined and sorted (*I, II* or *III*) according to the MPP related working point. Thus, that points determine the direction of the following update for duty cycle. The step size value will be selected in accordance with the specified above direction of the updated duty cycle. Forthat goal, the proposed MPPT response has been divided up into three regions and the working point zone could be specified (i.e. *I, II or III*).
Finally, depending on the region of working for the step size (*D*) has been updated.

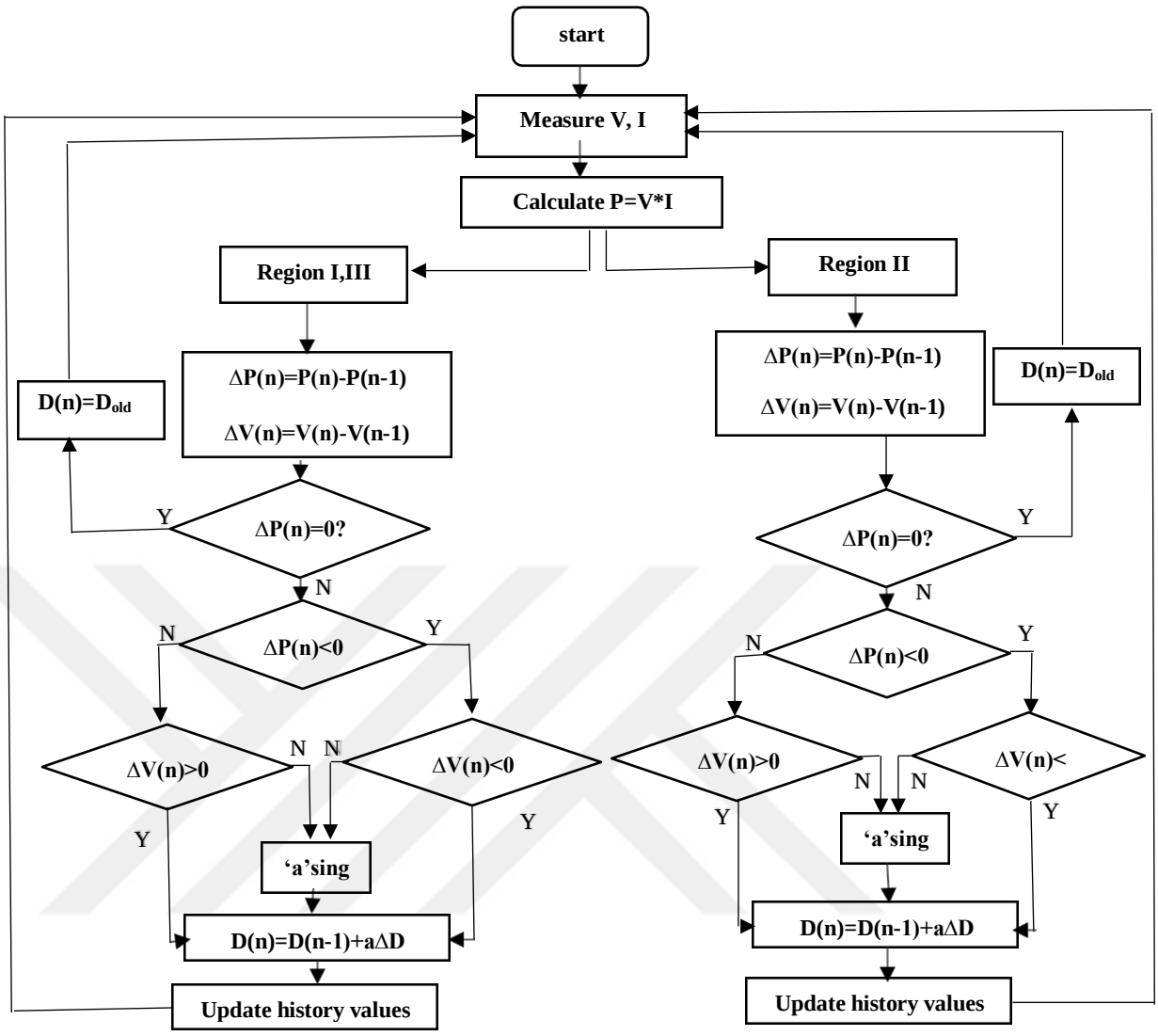

Figure 3.7 Proposed algorithm flowchart.

3.3 Boost converter circuit

The key principle that drives the boost converter is the tendency of an inductor to resist changes in current by creating and destroying a magnetic field. The circuit action during the initial high period of the high-frequency square wave applied to the MOSFET gate at startup. During this time MOSFET conducts, placing a short circuit from the right-hand side of L_1 to the negative input supply terminal. Therefore, the current flow from the positive to negative terminals of the supply through L_1. This stores energy in its magnetic field. There is virtually no current flowing in the remainder of the circuit as the combination of D_1, C_1, and the load represent a much higher impedance than the path directly through the heavily conducting MOSFET.

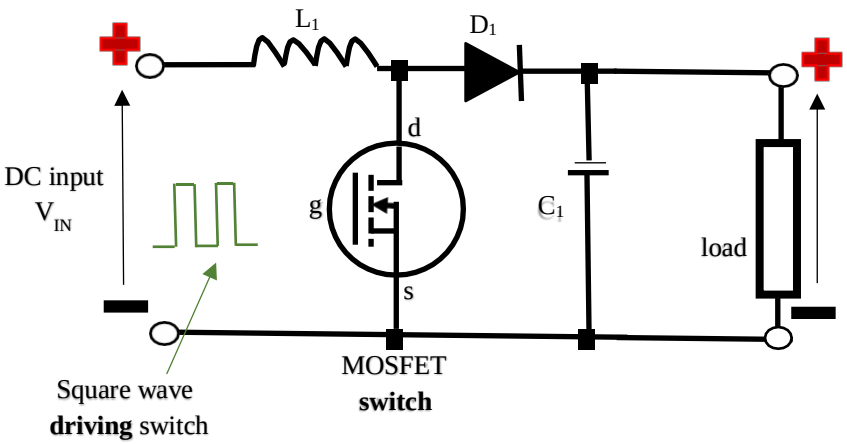

Figure 3.8 Boost converter circuit.

3.3.1 Current path with MOSFET Off

The circuit performs periodically during MOSFET after the initial start-up. Each time when the MOSFET conducts, the cathode of D_1 is more positive than its anode, due to the charge on C_1. The output of the circuit is isolated from the input. However, load continues to be supplied with $V_{IN} + V_L$ from the charge on C_1. Although the charge C_1 drains away through the load during this period, C_1 is recharged each time the MOSFET switches off. Thus, maintaining an almost steady output voltage across the load.

At Low wave, the circuit of the MOSFET is rapidly turned off and sudden drop in current occurred. Therefore, the magnetic field is released back into the coils of the inductor. The stored energy appears in the form of voltage across the inductor, but with opposite polarity to the original applied voltage. This results in two voltages, the supply voltage V_{IN} and V_L across L_1. The resulting current through D_1 charges up C_1 to $V_{IN} + V_L$.

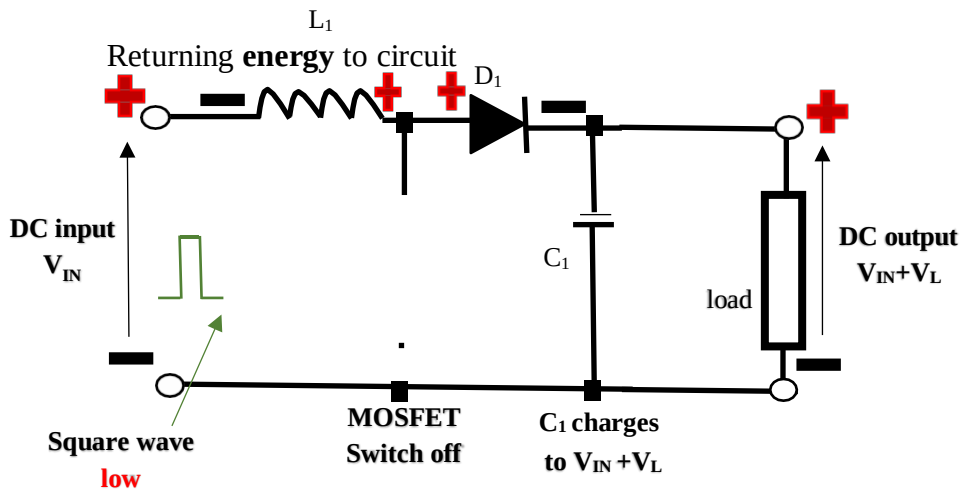

Figure 3.9 Current path with MOSFET off.

3.3.2 Current path with MOSFET ON

During high wave, the circuit of the MOSFET makes short circuit. Therefore, a current flow between the positive and negative supply terminals through L_1, which stores energy in its magnetic field. The circuit performs during MOSFET on periods after the initial start-up. Each time the MOSFET conducts, the cathode of D_1 is more positive than its anode, due to the charge on C_1. The output of the circuit is isolated from the input; however, the load continues to be supplied with $V_{IN} + V_L$ from the charge on C_1. Although the charge C_1 drains away through the load during this period, C_1 is recharged each time the MOSFET switches off, so maintaining an almost steady output voltage across the load.

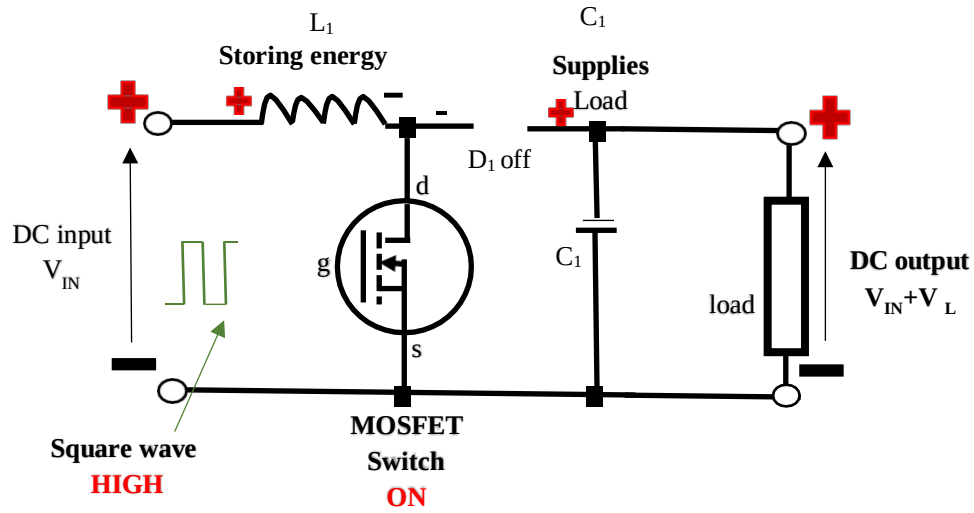

Figure 3.10 Current path with MOSFET on.

We obtain the current through the inductor using the following formulas:

- Switch closed for DT seconds:

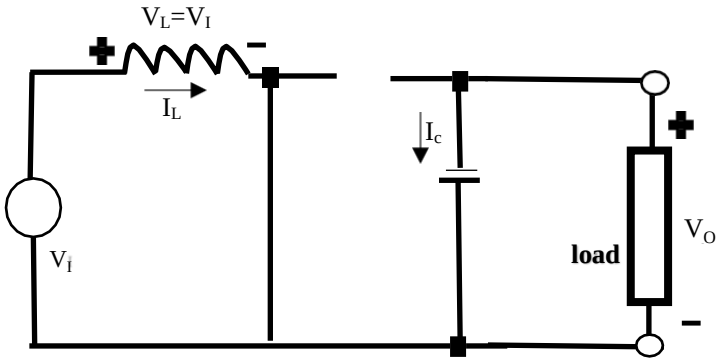

Switch on

0<t<DT

$$V_s = L\frac{di_L(t)}{dt}$$

$$i_l(t) = \frac{V_s}{L}t + c$$

$$\Delta i_L(ON) = \frac{V_s}{L}DT$$

Figure 3.11 Boost circuit when Switch closed for DT seconds.

- Switch open for (1 − D)T seconds:

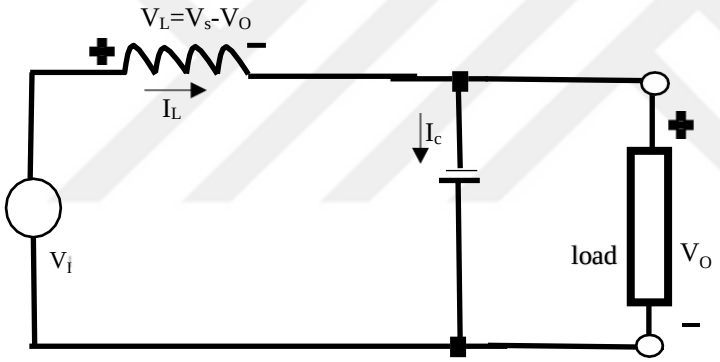

Switch off

DT<t<T

$$V_s - V_o = L\frac{di_L(t)}{dt}$$

$$i_L(t) = \frac{V_s - V_o}{L}t + c$$

$$\Delta i_L\ (OFF) = \frac{V_s - V_o}{L}(1 - \ )T$$

Figure 3.12 Boost circuit when switch open for (1 − d) t seconds.

The theoretical *DC* output voltage is determined by the input voltage (V_{IN}) divided by 1 minus the duty cycle (D) of the switching waveform, so the bigger the duty cycle gets, the higher will be the output. The duty cycle of the *PWM* can have values between 0 and 1. Therefore, the only possible output will be equal or higher than the input. That's why this configuration is called a step-up converter.

$$\Delta i_L\ (ON) + \Delta i_L\ (OFF)$$

$$\frac{V_s}{L}DT + \frac{V - V_o}{L}(1 - D)T \qquad (3.5)$$

$$V_O = \frac{1}{1 - D}\ V_S$$

3.4 Summary

The suggested MPPT algorithm has been illustrated, discussed, analyzed and discussed comprehensively in this chapter. A modified method to update the duty cycle is proposed. Moreover, the designed algorithm flowchart and DC-DC boost converter circuit have been comprehensively illustrated and analyzed.

CHAPTER 4

PCB DESIGN / RESULTS OF EXPERIMENTAL AND SIMULATION

4.1 Preface

We will discuss a practical simulation of the proposed algorithm and the results will be validated in this chapter. Simulation results have been obtained according to global standard-conditions. Therefore, comparison have been done with echo of *P* and *O* algorithm. In addition, the dynamical response of the proposed algorithm have been examined through various scales of solar radiation. Moreover, utilizing STM microcontroller (which is the most developed microcontroller) with DC-DC boost converter, printed circuit board (PCB), which represents the electronic prototype has been achieved. Experimental result and analysis of the electronic card schematic and all design parameters will be shown as well.

4.2 Simulation System

4.2.1 PV Module

The module of PV has been designed and simulated with current-voltage gates, and to make the comparison of various solar radiation scales, we added solar radiation and solar radiation gates as well. To know the (*V-I*) properties of the PV module, we may identify four values of parameters. And it is always given in PV module's datasheet i.e., 1) V_o represents the voltage of open-circuit, 2) I_s represents the current of short-circuit, 3) V_m represents the maximum voltage, 4) I_m represents the maximum current. The PV module has been designed to match the panel that we used in experimental test, therefore, these parameters are considered: $V_o = 21.9V$, $Is = 5A$, $V_m = 17.7V$, and $I_m = 4.52A$ (as written in datasheet).

In the standard conditions where solar irradiation is *1000 watt/m2* and temperature is set to *25°C*, the current is set off from *0* until *Is* (short circuit current) which feeds the PVmodule.

The comparison between the proposed *P* and *O* and the normal *P* and *O* algorithm will be verified using the above-mentioned PV module.

4.2.2 Design of DC-DC Boost Converter

DC-DC Boost Converter theory is applied to use its circuit in the simulation test. The equation and parameters of DC-DC Boost circuit have been clarified in Equations (4.1)-(4.3) [22]. L1 represents the inductor coil, and its rate have to be as large as we possible to obligate boost converter working at permanent style. Therefore, mathematically it can be written as:

$$L_1 \geq \frac{V_{om}(1-D_{mp})}{F_s|\,\Delta I_L|} \tag{4.1}$$

C_1 represents the capacitor output, and its rate has to be designed to catch minimum output V_r (voltage-ripple). Therefore, mathematically it can be computed as:

$$C_1 \geq \frac{D_{mp} I_{om}}{r f_s v_{om}} \tag{4.2}$$

While r represents the factor of ripple, I_{om} represents the max output current of DC components. Therefore, mathematically it can be written as

$$r = \frac{\Delta V_O}{V_{om}} \tag{4.3}$$

The selected parameters of DC-DC boost converter circuit are obligating boost converter working at permanent style. Therefore, the ripple in produced voltage is lower than 2%, the ripple in incoming current is lower than 2%, and the ripple of inductor's current from climax to climax is 0.05A. After calculating all rates via Equations (4.1) - (4.2), L_1*=1mH,* C_1*=220uF,* R*=1Ω,* and F_s is *5 KHz* (which represents the converting frequency).

4.2.3 Entire Simulation

The Entire PV system's simulation is illustrated at Figure 4.1. The illustration contains essentially the PV module, DC-DC boost converter after that load. Moreover, to verify the proposed algorithm it includes a *P* and *O* MPPT box. Last component has been placed to show the produced outcomes, that is multiple entries scope. As it noticeable that the voltage and current are coming from panel and enter to the *P* and *O*

MPPT box (where the power is calculated). These inputs are then fed to MPPT Algorithm box which samples the voltage and current periodically on a pre-set sampling frequency of 5 *KHz.* The block processes the voltage and current data using the built-in function of the proposed algorithm (Sampling time is $5* 10^{-6}$).

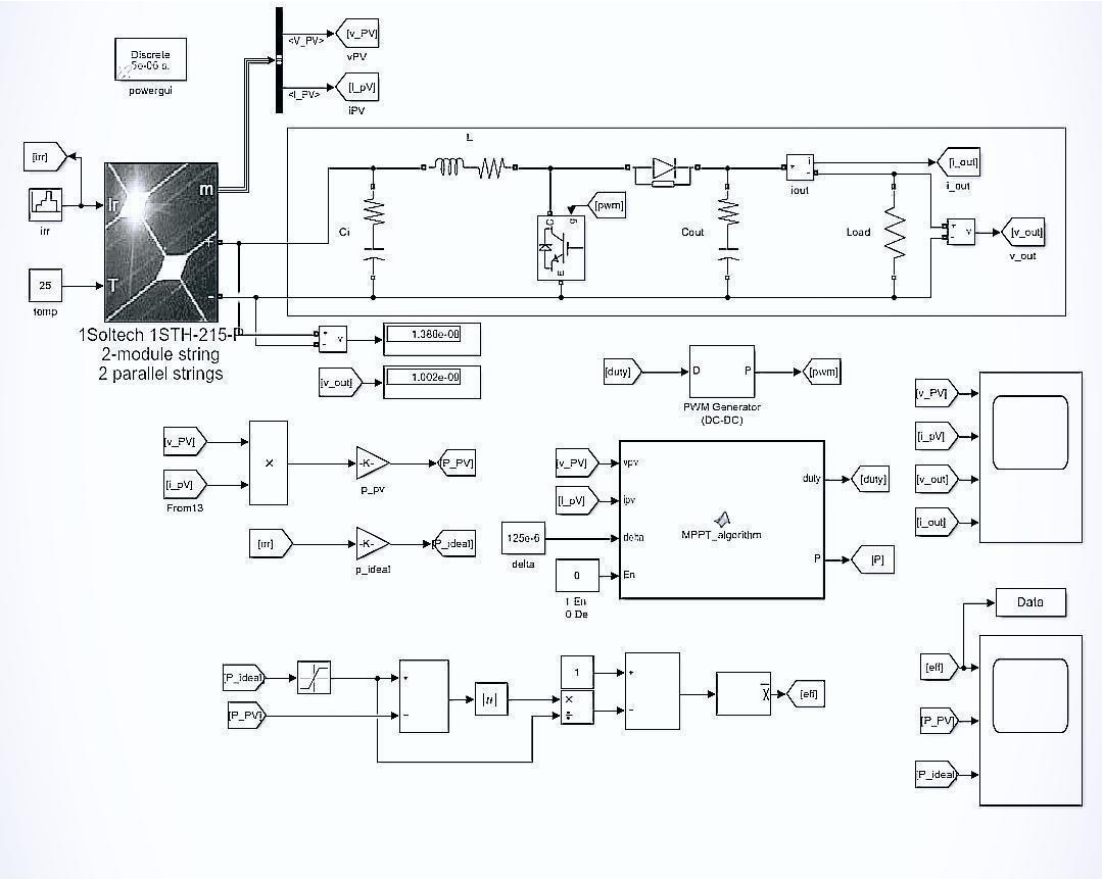

Figure 4.1 Entire PV system's simulation.

Even after the duty cycle is selected as reference (in MPPT algorithm box), the PWM represents output of *P* and *O* MPPT box (after passing the PWM generator which converts the duty cycle to PWM). After that PWM enters to boost circuit to make controlling in circuit. The panel's produced voltage is entering to boost circuit and addressed depending on duty cycle. In order to compute the produced current I_o of a boost circuit, we can find its value across the produced voltage V_o as follows.

$$I_0 = \frac{V_0}{R} \tag{4.4}$$

To enhance the efficiency of the circuit to achieve ideal power, an additional circuit has been also added.

4.3 Temporary/Permanent Respond Case

As we mentioned previously that the simulation of proposed algorithm has been implemented with standard conditions (*1000W/m2* and *25°C*). In order to produced power of panel (*Pm = 80.004W*), the PV module's parameters are V_{oc}*=21.9*, I_{sc}*=5A*, V_{mp}*=17.7V* and I_{mp}*=4.52A*.

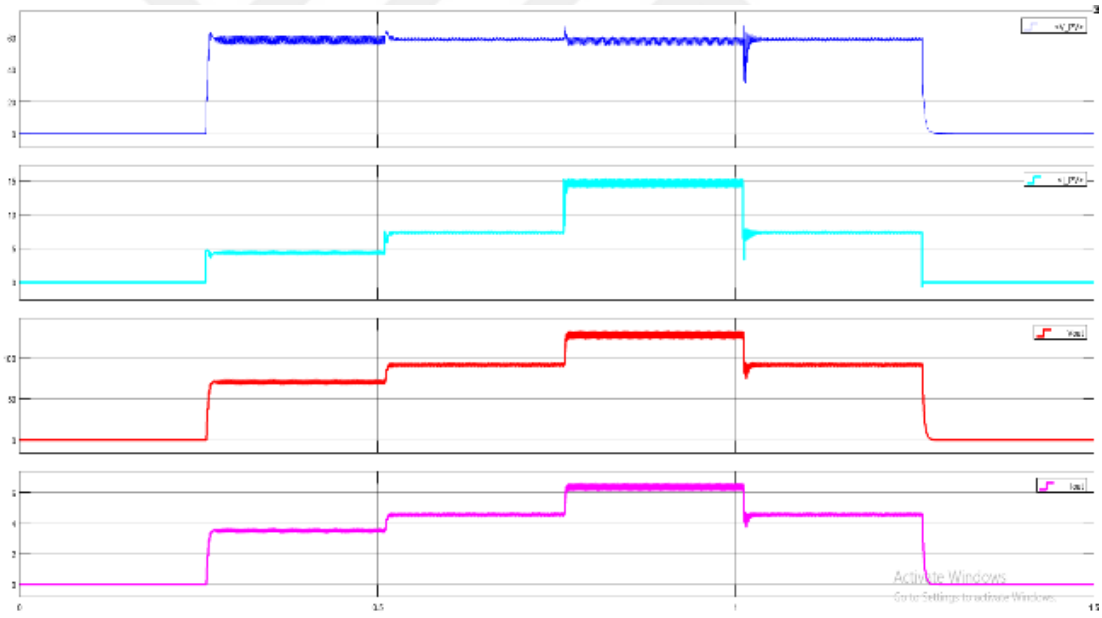

(A)

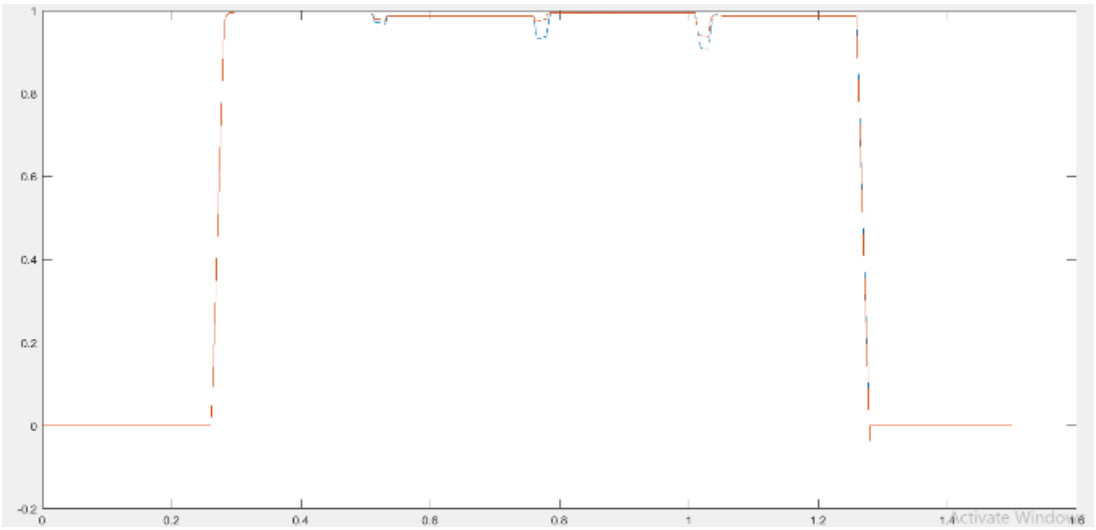

(B)

Figure 4.2 Results of PV system: (A) simulation of I, V. (B) simulation of efficiency.

The selected first rate of the duty cycle is sufficiently away of maximum duty cycle. One can notice that in time period ($t < 3ms$), the proposed algorithm has ability to specify the functional field (zone1). Moreover, depending on Equation (3.4), the step size will be refreshed. In zone 1, large step size has been selected till reach zone 2. In zone 2, step size turned to D_2, small one till achieving MPP. The top power value has been accomplished in *4ms*. At the period $(4 < t < 10)$ ms, the functional point is oscillatingin zone 2 as shown in Figure 3.5. The step size rate has been adjusted to lowest value at this period of time, while the functional point occur in this zone.

4.3.1 Differentiation of *P* and *O*

In order to estimate the implementation and efficiency of proposed algorithm, first of all, comparison was done between the results of the proposed algorithm and normal *P* and *O* algorithm. The comparison process is carried out in such a way that there is compatibility between the step size and the duty cycle.

The respond of normal *P* and *O* has been differentiated and shown with proposed *P* and *O*. Consequently, the typical state of error is shown for both of them, while mean error is computed for differentiation objectives. Simulation results are obtained according to global standard-conditions (*1000W/m2, 25°C*) and demonstrated in Figure 4.3. Running time of simulation is 1.5 second, which aimed to validate the betterment at temporary/permanent Respond Case of proposed *P* and *O* (where: A

represents the normal algorithm, B represents the proposed algorithm and the amount of improvement).

As shown in Figure 4.3, it is noticeable that the proposed P_{pv} follows ideal P_{pv} at different radiation levels to show the improvements in efficiency while the solar panel working in changeable weather conditions. The reactions of both algorithms are shown in Figure 4.4. In *25ms* the maximum power has been achieved in *P* and *O* at the first irradiation. The maximum aimed power chosen at the simulation situations is *80.004W*. After adjustment, the error is computed.

In the small duty cycle case, the error rate among the typical reaction and (*P* and *O*) reaction is illustrated in Figure 4.5 (a), that the mean error is computed to be *0.3944*. The error rate among the typical outcomes and the proposed *P* and *O* reaction is shown in Figure 4.5 (b), that the mean error is computed to be *0.1857*. That is led to betterment in the efficiency about *31.35%*. This is the temporary (passing) respond. In the case of small step size, the *P* and *O* results in slowly temporary respond. However, constant steady-state reaction and respond may be obtained.

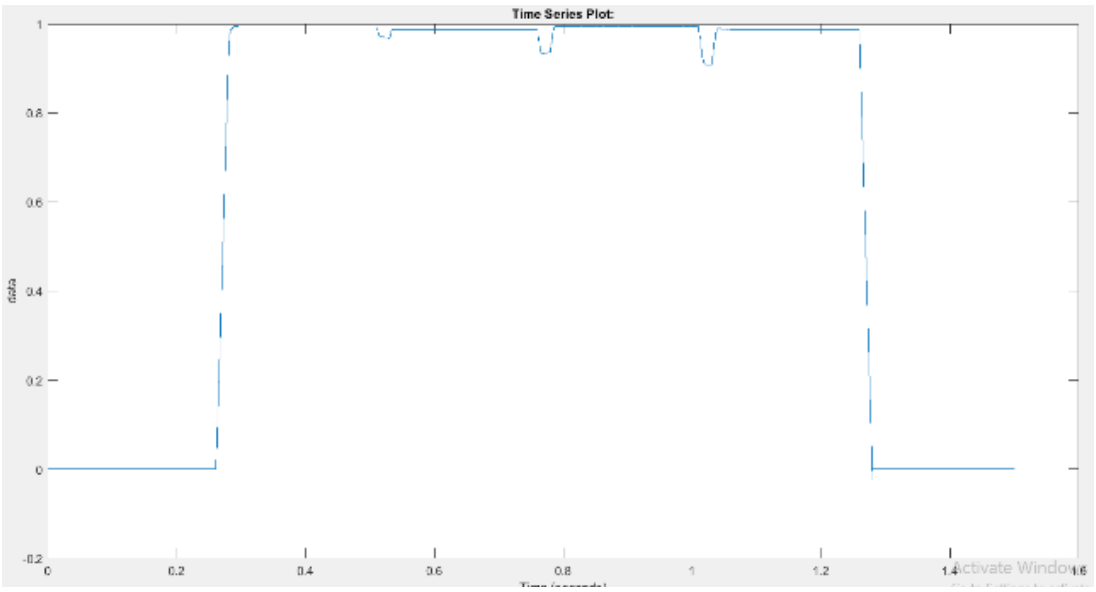

(A)

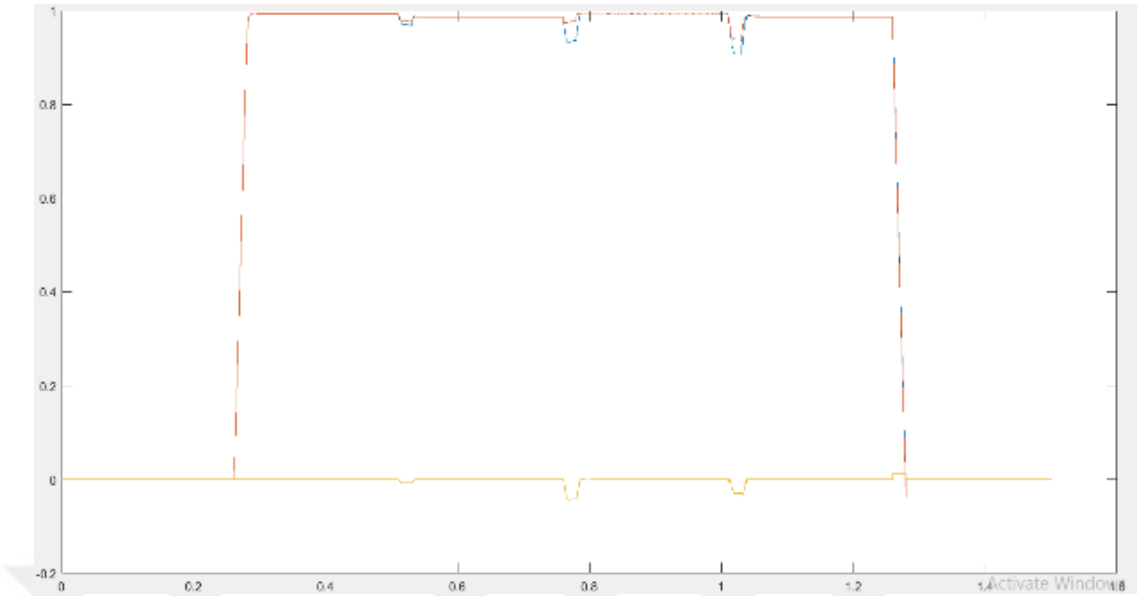

(B)

Figure 4.3 The differentiation: (A) normal algorthim, (B) proposed algorithm.

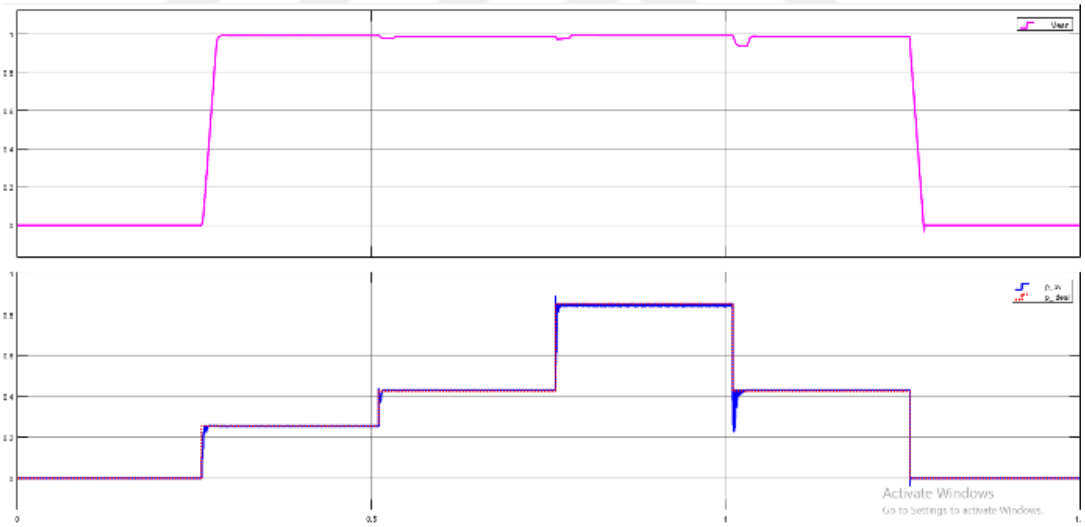

Figure 4.4 Efficiency comparison of proposed P_{pv} with Ideal $P_{pv.}$

In the large duty cycle case, the error rate among the typical reaction and (P and O) reaction is given in Figure 4.6 (a). Where the mean error is computed to be 0.2129. The error rate among the typical outcomes and the proposed P and O algorithm is shown in Figure 4.6 (b).

From which the mean error is computed to be *0.1857*. That is led to betterment in the efficiency about *4.09%* that means important betterment in the steady-state reaction and respond, results in considerable earn over in the long-term. The constant step size in the *P* and *O* leads to a late temporary reaction and respond (if duty cycle is small) but a stable steady-state response and vice versa. However, the achievements of both small and large step size of normal (*P* and *O*) could be verified by proposed *P* and *O*. In addition, stable steady-state reaction and respond at same time.

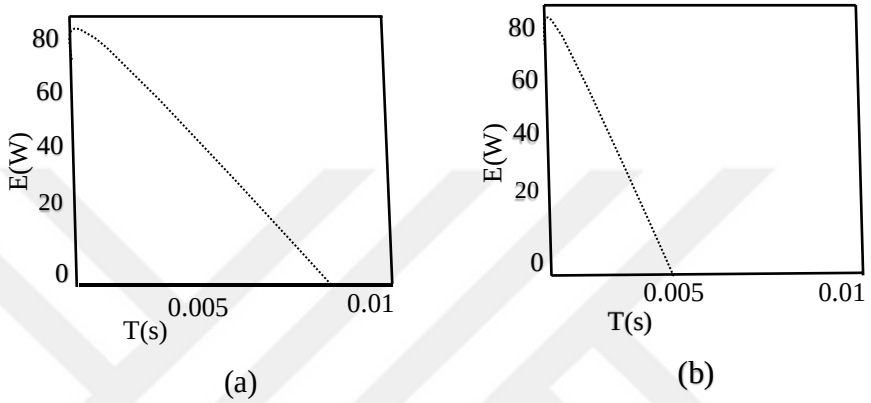

Figure 4.5 The error rate: (a) typical state, (b) proposed algorithm.

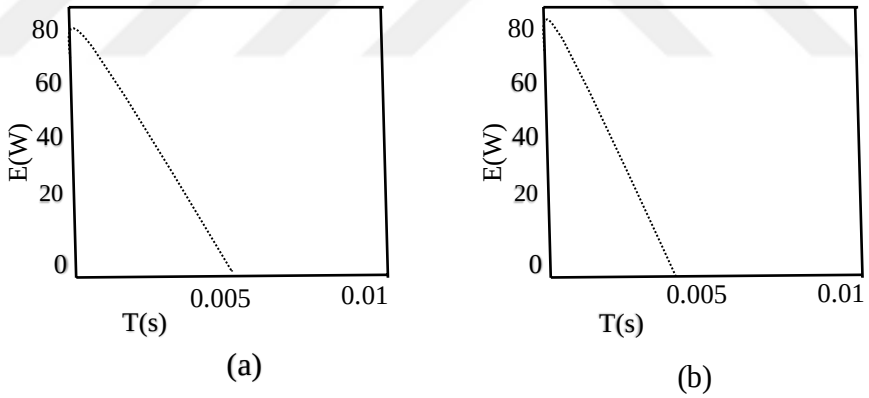

Figure 4.6 The error rate: (a) typical state, (b) proposed algorithm.

4.4 Outcomes and Debates

In this section, the dynamical respond of the presented algorithm will be examined through various scales of solar radiation; comparison of result will be done with normal *P* and *O* algorithm.

Table of comparison is computed to show directly the usefulness of the proposed (*P* and *O*) algorithm. The efficiency is also calculated with the proposed (*P* and *O*), and a normal (*P* and *O*) utilizing fixed step. In Table 4.1, the computed values of output

power at load and the maximum power that can be delivered by the solar panel are shown. A comparison is done between the output power of proposed (*P* and *O*), and a normal (*P* and *O*).

Table 4.2 Comparison between maximum power of proposed solar module P and O, and a normal P and O.

Solar Insolation	Output Power Proposed P and O	Output Power Normal P and O
200	**169.9**	**157.5**
300	**258**	**242.9**
600	**520.6**	**485.1**
1000	**891.3**	**856.1**

The waveforms at insolation of *200*, *300*, *600* and *1000* of proposed (*P* and *O*) and a normal (*P* and *O*) are demonstrated in Figures 4.7 – 4.14. The Unit of insolation is W/m^2. So, it is considered that at *200*, *300*, *600* and *1000* values of input *200*, *300*, *600* and *1000* W/m^2 insolation is provided.

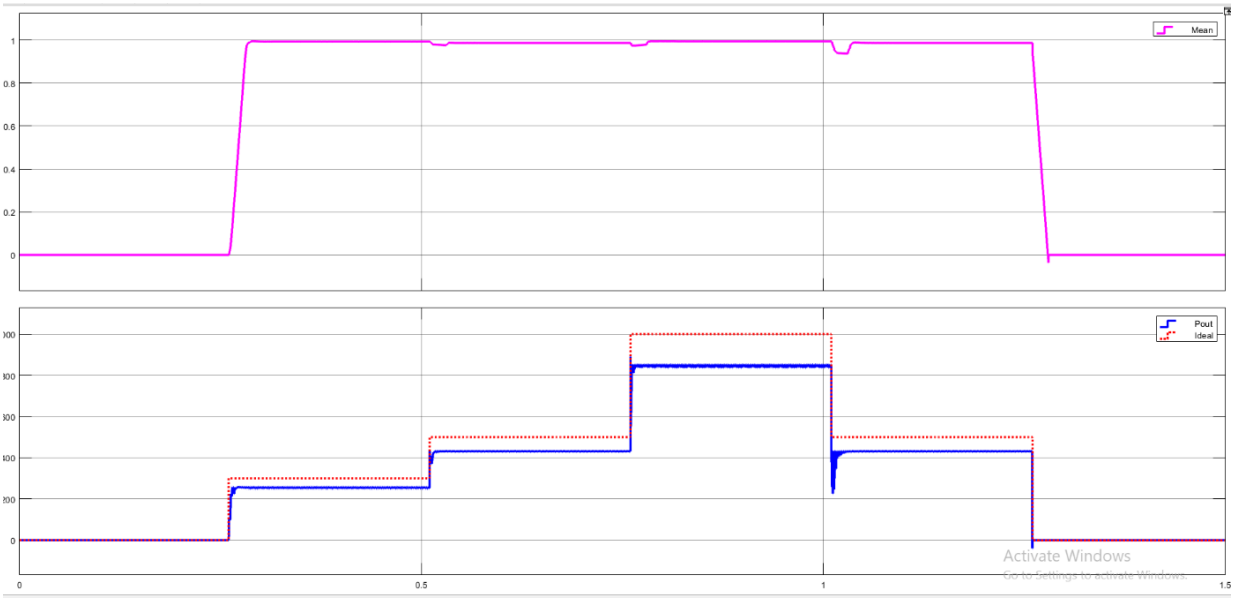

Figure 4.7 Maximum power by PV module at insolation 1000 with proposed *P* and *O*.

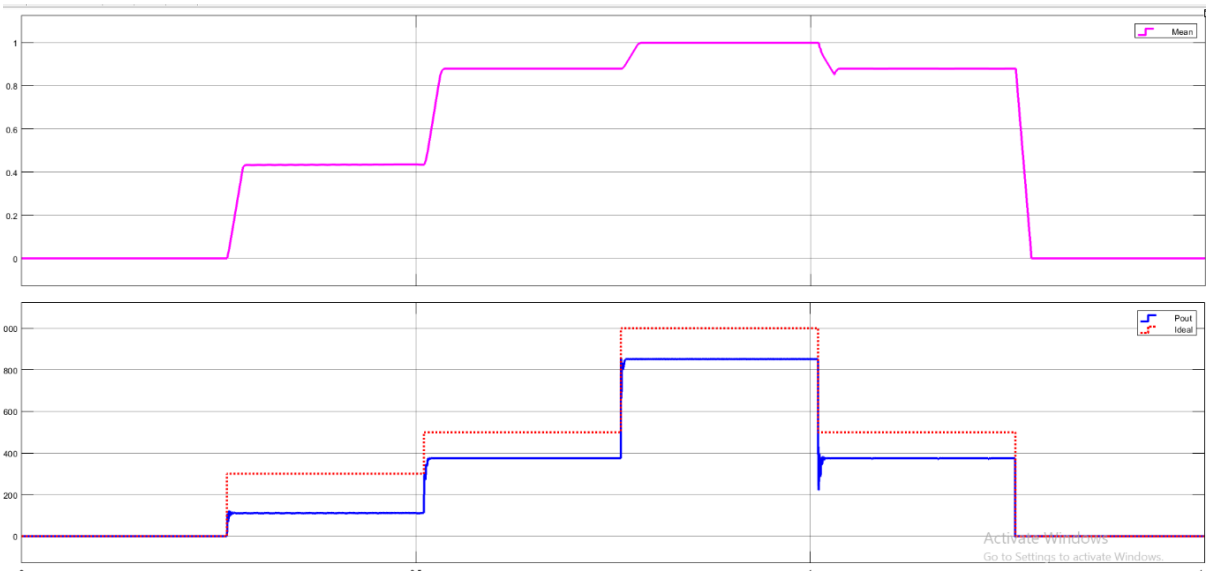

Figure 4.8 Maximum power PV module at insolation 1000 with normal *P* and *O*.

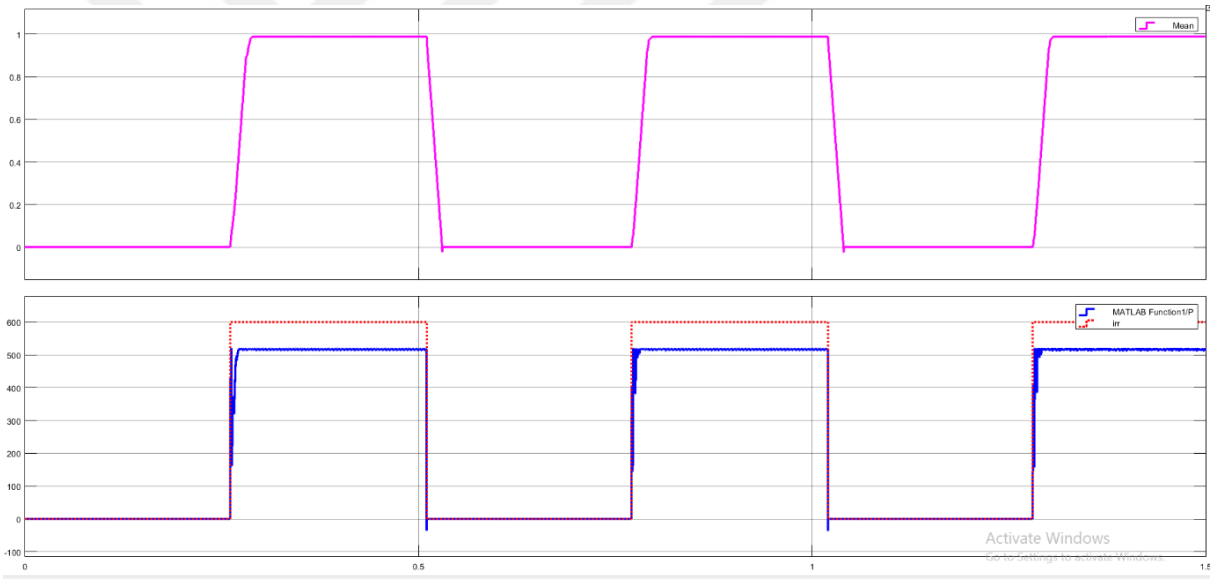

Figure 4.9 Maximum power PV module at insolation 600 proposed P and O.

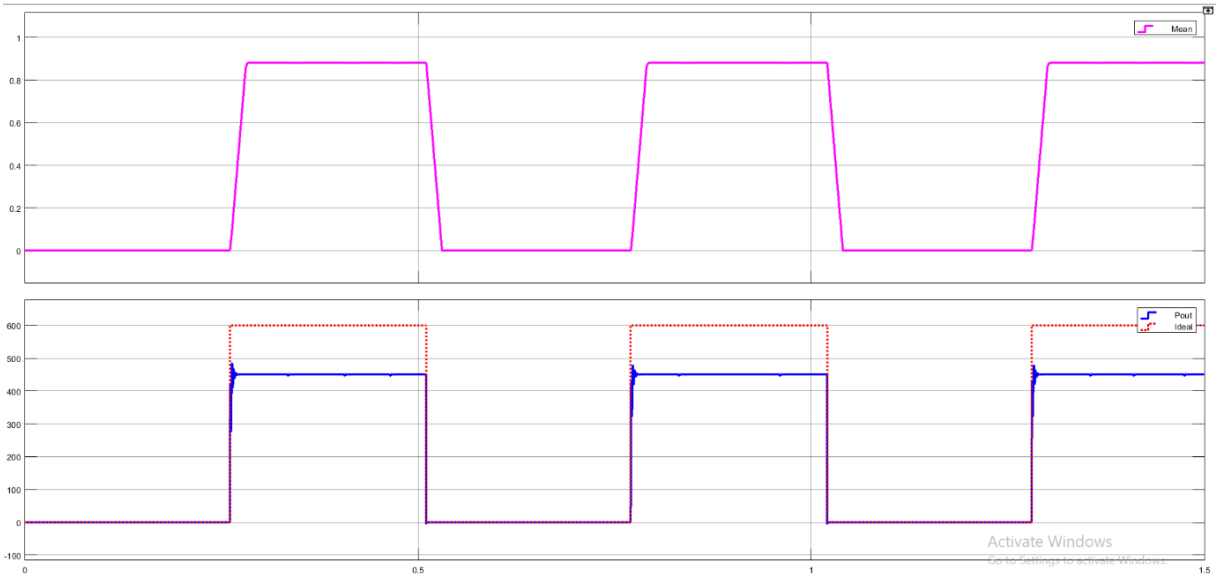

Figure 4.10 Maximum power PV module at insolation 600 normal P and O.

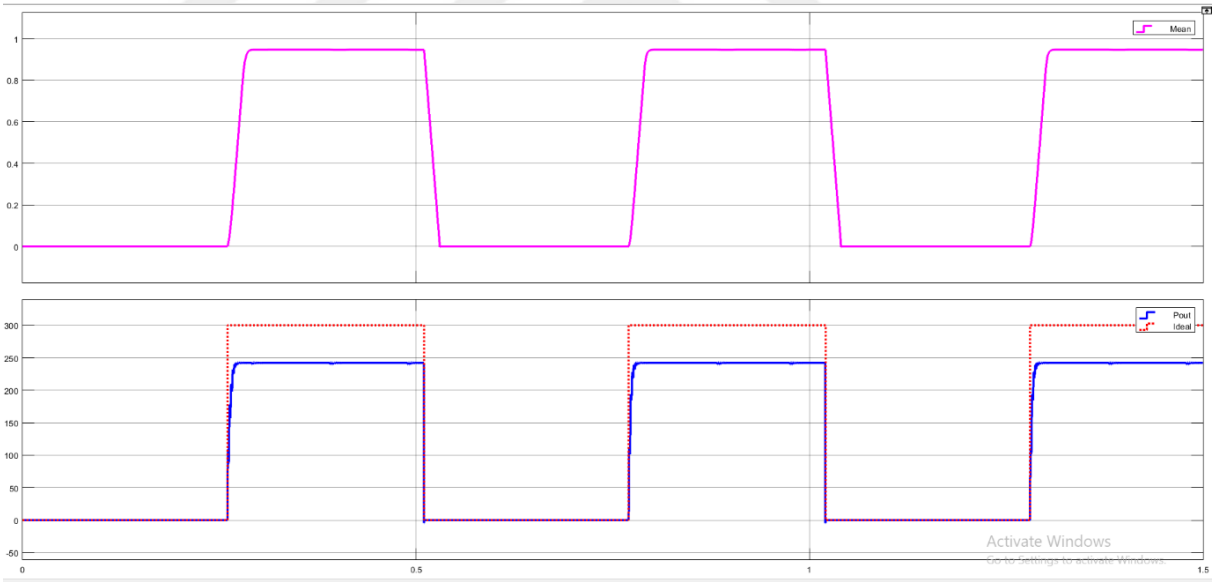

Figure 4.11 Maximum power PV module at insolation 300 normal P and O.

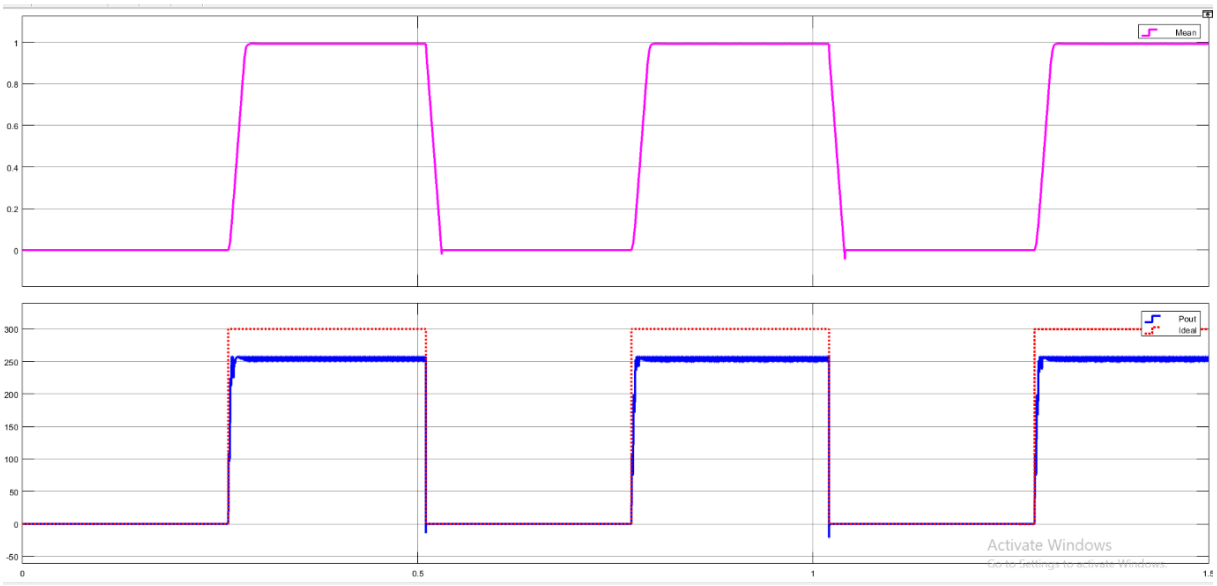

Figure 4.12 Maximum power PV module at insolation 300 proposed P and O.

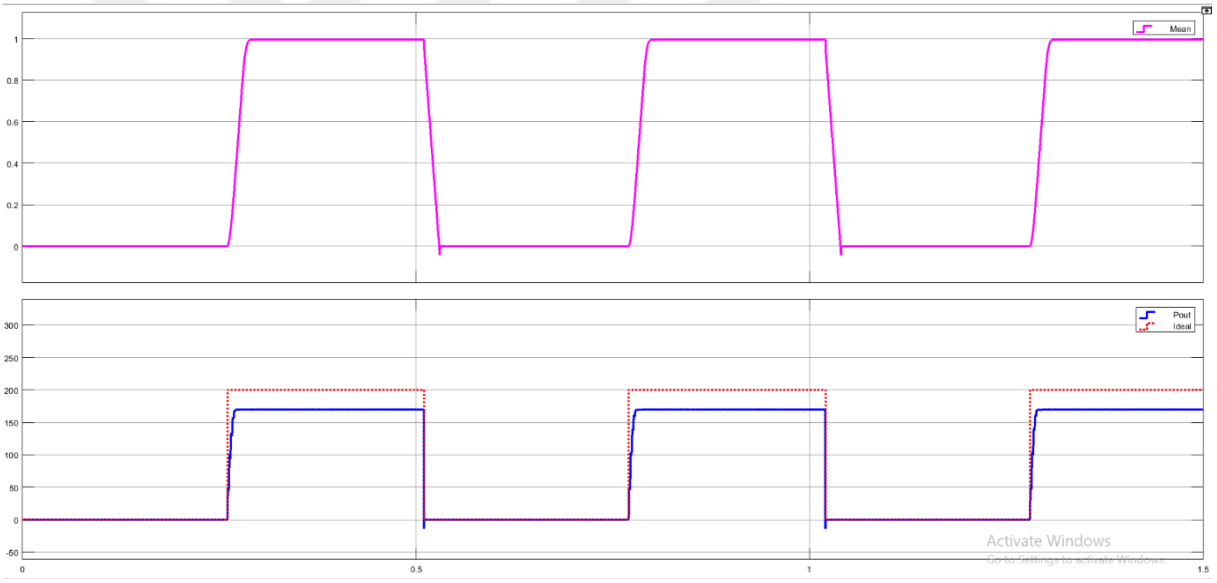

Figure 4.13 Maximum power PV module at insolation 200 proposed P and O.

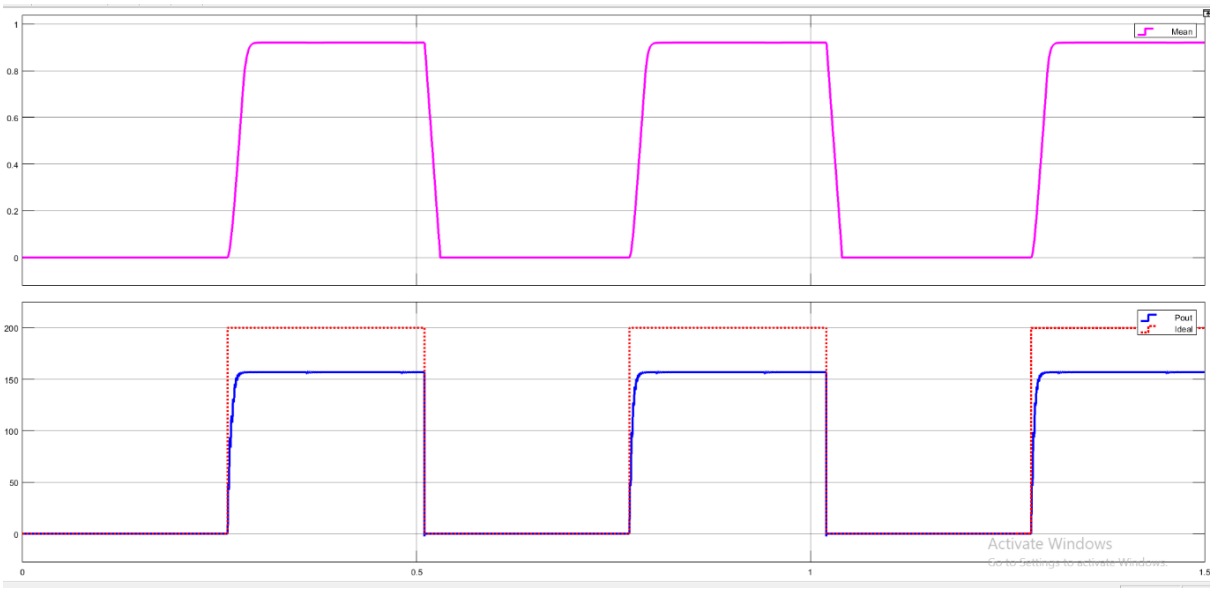

Figure 4.14 Maximum power PV module at insolation 200 normal P and O.

In Table 4.2, the efficiencies of the Photovoltaic system are compared between the proposed (*P* and *O*) and a normal *P* and *O*. It can be seen from Table 4.2, the efficiency comes out to be *98.88– 99.45*, which is a very good range in comparison to the efficiency of normal (*P* and *O*) algorithm [19].

The following formula was used to calculate efficiency at a particular insolation [23]:

$$Efficiency = \frac{Power\ at\ Load}{Maximum\ Power\ given\ by\ Solar\ Module} \tag{4.5}$$

Table 4.3 Computed efficiency values for proposed and a normal *P* and *O*.

Solar Insolation	Proposed P and O	Normal P and O
200	**99.56**	**92.04**
300	**99.44**	**94.68**
600	**98.88**	**91.85**
1000	**99.45**	**98.54**

The computed values show that the MPPT circuit enhances the power extraction capability of the load by tracking MPP quickly with using STM32 Microcontroller. Also, the proposed (*P* and *O*) conductance algorithm is very useful and accurate.

4.5 Experimental Design and Test

4.5.1 Comprehensive Schematic of Hardware Parts & PCB Design

A comprehensive schematic diagram of hardware parts and design has been illustrated in Figures 4.15 and 4.16. The electronic card circuit that is connected to PV panel and has DC-DC boost converter, STM microcontroller, sensors for current and voltage, and some other parts to secure the durability of the PV system.

Sensors connected to the solar panel were used to sense the value of voltage and current coming from the solar panel. To compute the values of V_p and I_p, samples are taken out. Then the signals are transmitted to low pass filters (LPF) to make the signal quality better and to get rid of unwanted parts of the signals.

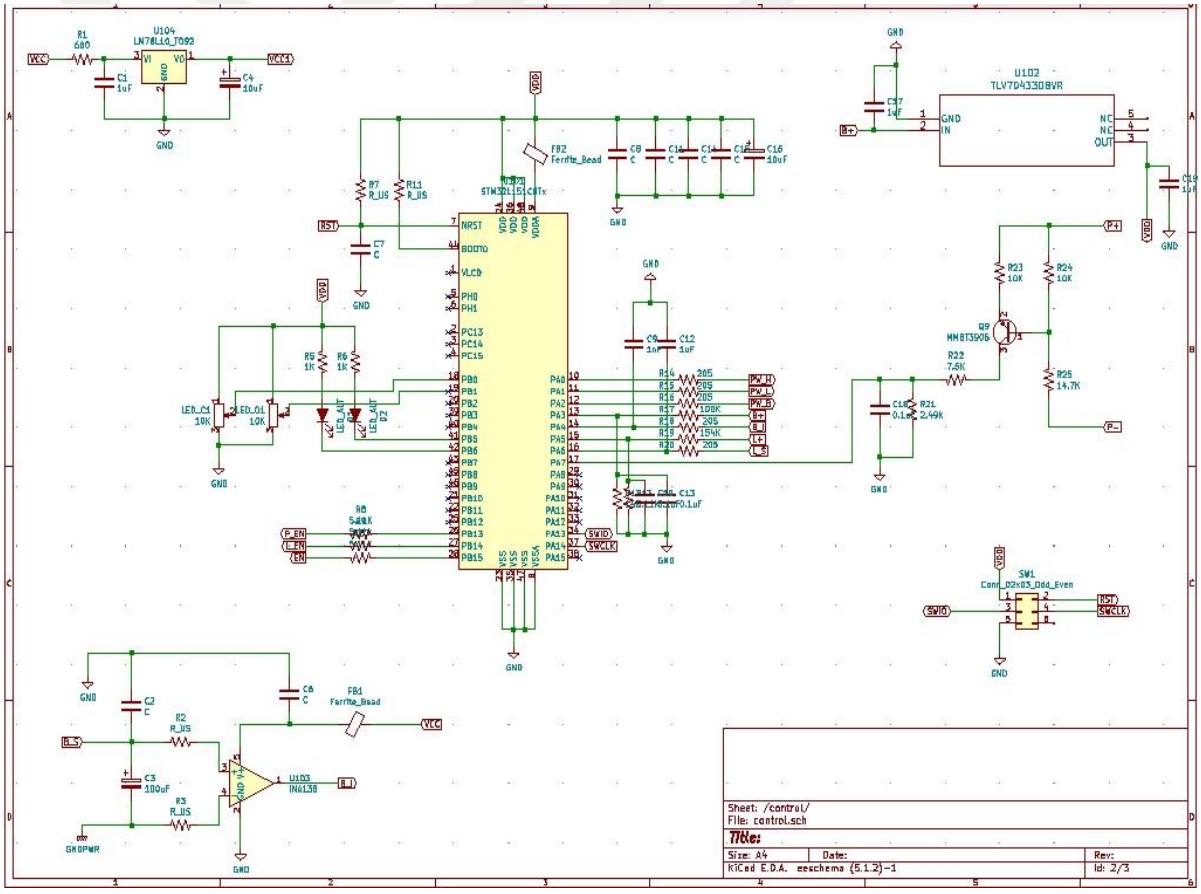

Figure 4.15 Downer layer of circuit.

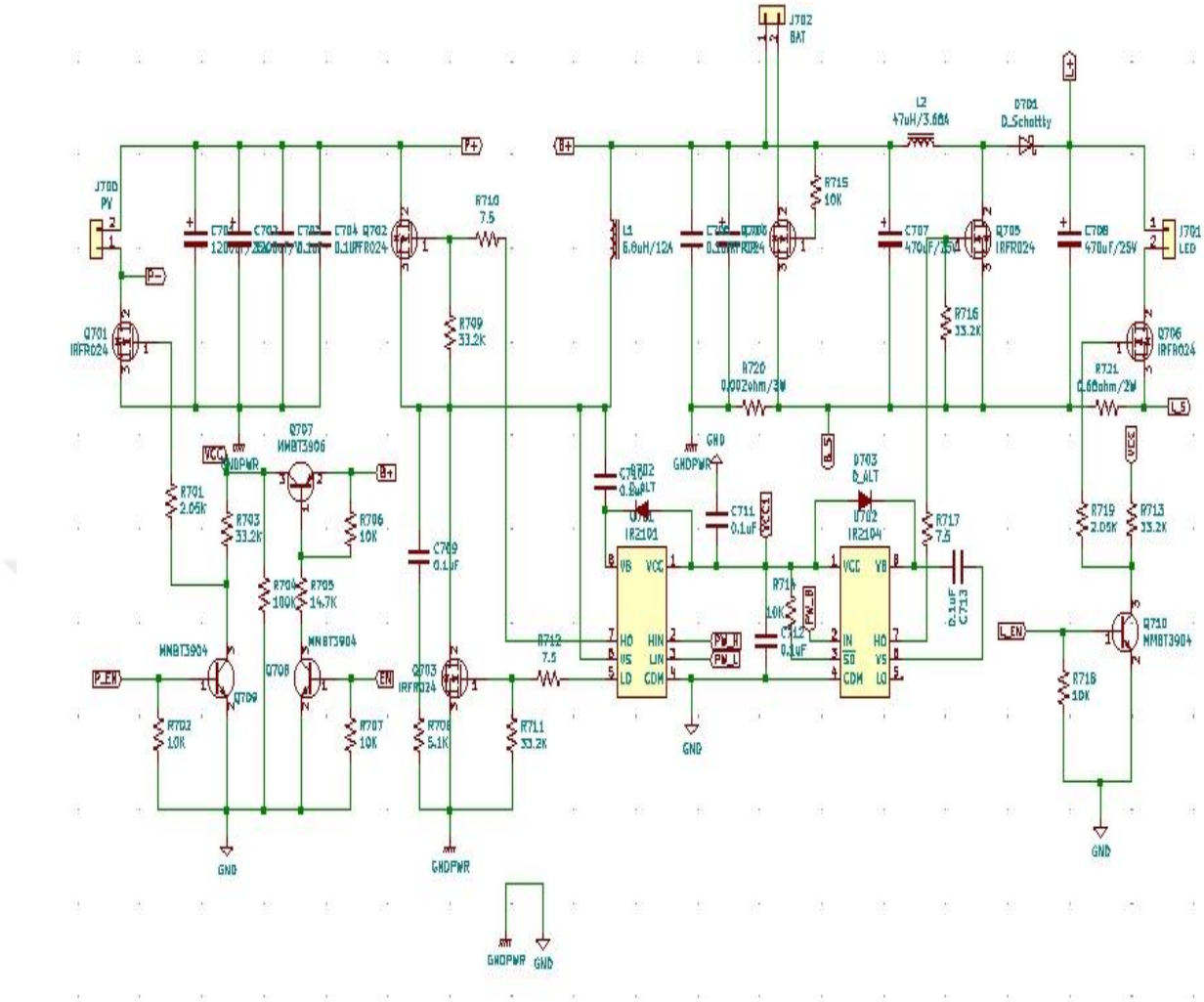

Figure 4.16 Upper layer of circuit.

Consequently, the analogy/digital pins which exist in STM microcontroller receive these signals and convert them to digital signals. The most important operation of STM microcontroller is to receive the V_p and $I_{p,}$ then compute and determine the step size and direct the orientation. Finally, PWM signal comes up from STM microcontroller and enter to DC-DC boost converter circuit.

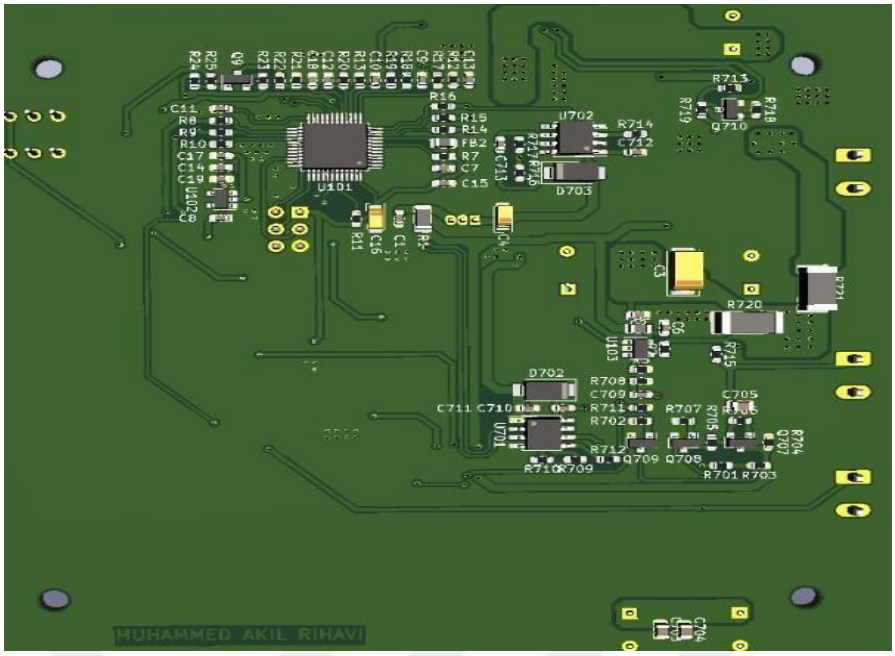

Figure 4.17 Downer layer of PCB.

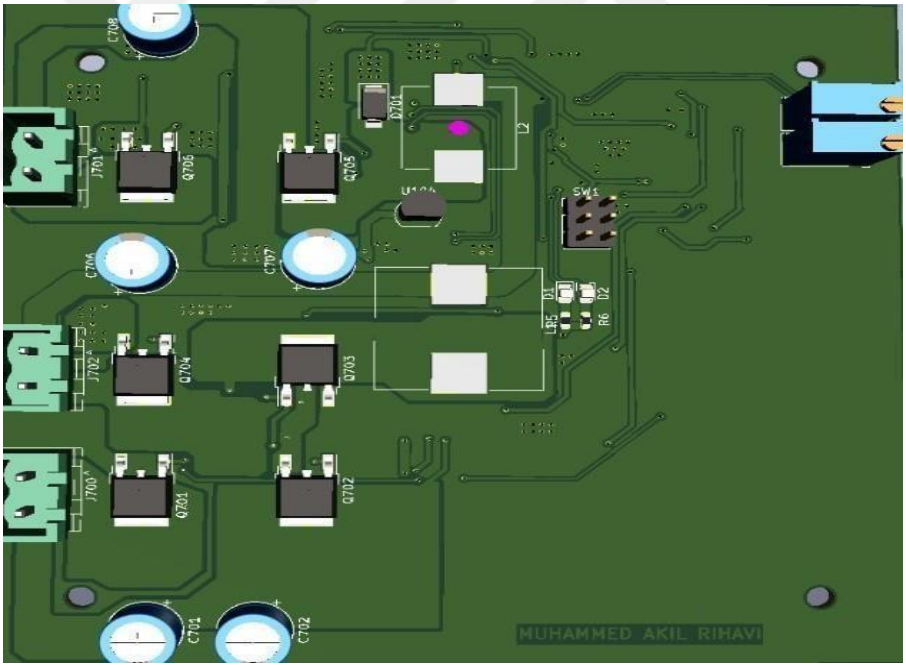

Figure 4.18 Upper layer of PCB.

Global standard exam situations have been shown in Table 4.3. In addition, datasheet contains the voltage-current (*V-I*) features and voltage-power (*V-P*) features of applied module. A comprehensive layout of hardware parts and design has been manifested in Figures 4.17 and 4.18.

Table 4.3 The specifications of the PV modules.

Parameters	Variable	Value	Unit
Short-circuit current	I_{SC}	5	A
Open circuit voltage	V_{OC}	21.9	V
Current at maximum power point	I_{MPP}	4.52	A
Voltage at maximum power point	V_{MPP}	17.7	V
Maximum power	P_{MPP}	80.004	W
V_{OC} coef, of temperature	K_V	-0.32	V\°C
I_{SC} coef , of temperature	K_I	0.04	A\°C
No. of modules in series (per string)	N_S	1	–
No. of parallel strings	N_P	1	–
Light-generated current I_L	I_L	5.0238	A
Diode saturation current I_0	I_0	$3.6974e^{-11}$	A
Shunt resistance R_{sh}	R_{sh}	70.2892	ohms
Series resistance R_s	R_s	0.35567	ohms
Diode ideality factor	–	0.92596	–

4.5.2 Voltage and Current Sensors

Voltage separator is utilized to gain the voltage of panel. Due to high resistance and reduction, less amount of the current flows in the separator. Therefore, it is so significant parameters to reduce the losing in power. Voltage separator has been implemented to make the highest outcome voltage is *3.6 V*, and must not cross the highest V_p (module work voltage value as V_{oc}) to save the STM microcontroller that has a highest boundary for inward voltage as mentioned in datasheet (*1.65 - 3.6*)*V*. Shunt resistance is applied in order to sense the panel current with amplifier of differentiation, the voltage drop on both ends of the amplifier of differentiation gives the value of the current coming from the solar panel.

The resistor value was applied is minimum as potential (*0.002Ω*) and connected in sequence with panel to reduce the losing power in this electronic circuit. Amplifier of differentiation has been implemented (its gain) to make the highest outcome voltage that is *3.6V*, and must not cross the highest I_p (module work current value as I_{sc}).

4.5.3 DC-DC Boost Circuit

The essence of MPPT system is DC-DC boost circuit which steps up the voltage value to catch up the highest potential V_p (voltage of panel). The filter of DC-DC boost circuit (LC outside) has been implemented to obligate the DC-DC boost working at permanent style at minimum voltage outcome ripple (*<2%*). The equations and formulations utilized in DC-DC boost are also utilized in card and experimental test.

4.5.4 Configuration of STM Microcontroller

A STM32L151C8 microcontroller has been used in the proposed MPPT system. This STM microcontroller has ultra-low-power 32-bit MCU ARM-based Cortex-M3, 128KB flash, 16KB SRAM, 4KB EEPROM, LCD, USB, ADC, DAC, that includes whole indispensable and needful components to carry out and verify the experimental test. The pin out and links of STM microcontroller have been shown in Figure 4.19.

Using STM32CubeMX FIRMWARE where the configuration of STM microcontroller has been done. We activated 4 channel input and one channel output via GPIO, TIMER (*tm2, ch2*), and 4 analogue / digital (*A/D*) canals of STM have been utilized for the current and voltage of solar panel (V_p, I_p). The *A/D* resolution of STM is 12bits, and *A/D* processing time is *19.72us*. According to samples taking frequency of proposed system (that is 10 KHz), the *19.72us*, is comparatively small.

In order to monitor and adjust the duty cycle of DC-DC boost circuit strictly, the fast PWM has been applied in the MPPT system. The DPWM resolution could reach 12bit. The DPWM is selected because of the convert frequency and resolution rate are contrary commensurate. According to the datasheet of STM, F_{osc} represents the clock frequency of STM microcontroller, and PWM frequency is represented via F_{PWM}. The bigger the convert frequency the lower the losing in conversion. Therefore, it is significant. Since extra bits of DPWM resolution are crucial in order to adjust duty cycle in small step. The frequency of PWM which applied in the experimental electronic circuit was set at *98.039 KHz*. This results in a 7bit resolution. Thus, *1/27* (*0.0078*) is the lowest step size that could be accomplished.

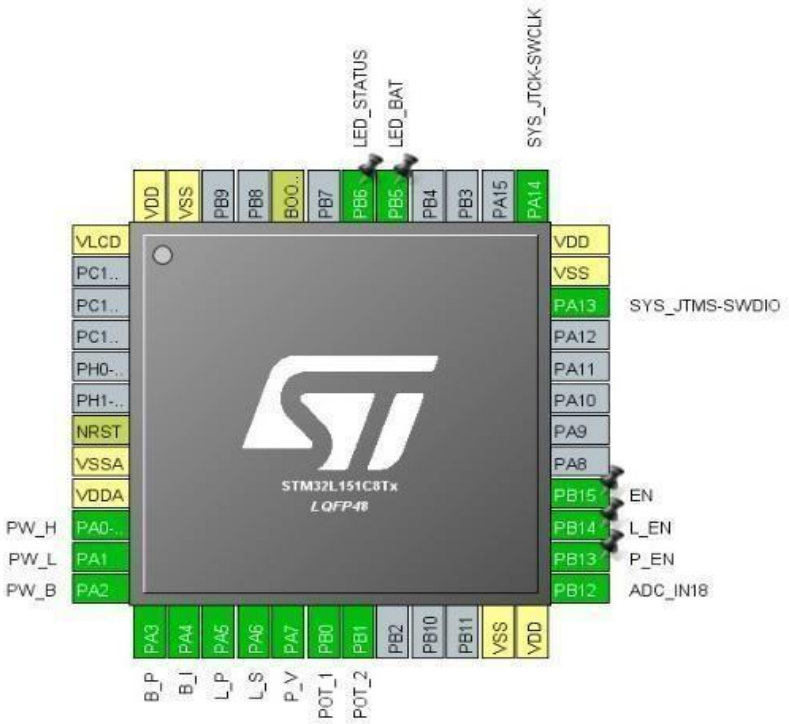

Figure 4.19 Configuration of STM32 microcontroller.

4.6 Outcomes of Experimental Test

An oscilloscope and power generator are applied and connected to the PCB circuit in the experimental test. The same rate of solar module which used in simulation test was applied. A few restrictions were faced in experimental test as: Artificial lights (sun simulation instruments), radiation measurement instruments, adjusting the radiation grades. Consequently, there was a small difference between the experimental and simulation outcomes. But, using STM microcontroller in the experimental test has given the ability to check out the operation process of suggested MPPT system. The results were recorded directly from oscilloscope (where *CH1* is voltage signal, *CH2* is current signal and *Math* is power signal). These results are also demonstrated in Figure 4.20. The output current and voltage (I_p ,V_p) have been listed cyclic (more than 500 samples). While the produced power was computed utilizing $P_o = V_o * I_o$.

The computed values of the suggested MPPT system are given in Table 4.4. In which (V_{in}, I_{in}, P_{in}) represent the panel parameters and (V_{out}, I_{out}, P_{out}) represent the output circuit parameters on load. Finally the efficiency in every radiation grade was computed.

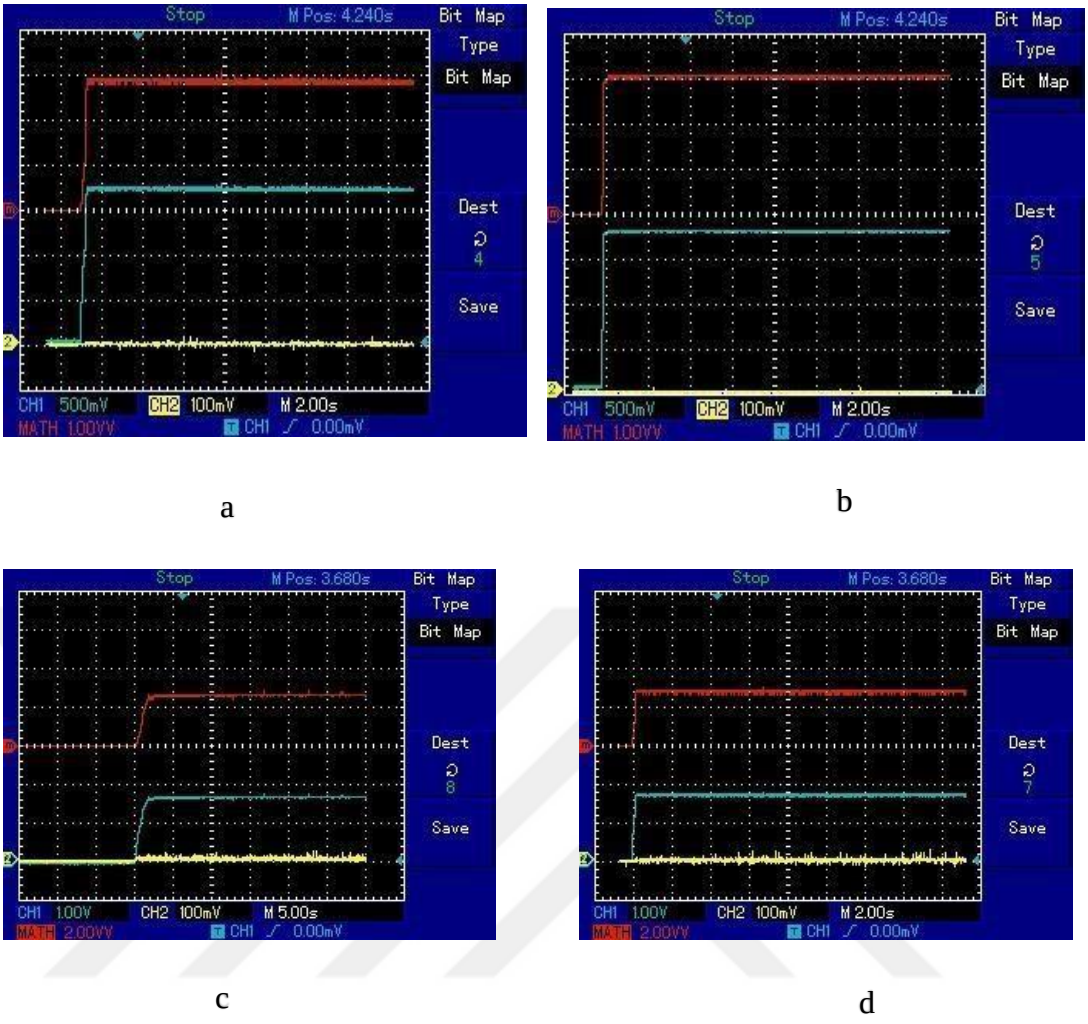

Figure 4.20 Results in oscilloscope with different insolation levels.

As one can see from Table 4.4, when the solar irradiation is *200 W/m²* the input voltage that is coming from the PV panel has a value of *15V* and the current coming from the PV panel has a value of *0.95A*.

The input power has a value of *14.25W*. While the output voltage value of the PV panel is *17.5V*, the output current value is *0.78A*, therefore, the output power is *13.65*W, and the percentage efficiency is *95.7*.v. When the solar irradiation is 600 *W/m²*, the input voltage that is coming from the PV panel has a value of 16*V* and the current out from the PV panel has a value of 2.6*A*, therefore, the input power has a value of 41.6*W*. While the output voltage value of the PV panel is *17.5V*, the output current value is 2.3*A*, therefore, the output power is 40.25, and the percentage efficiency is 96.8.

Table 4.4 Experimental results.

Solar Insolation	V_{in}	I_{in}	P_{in}	V_{out}	I_{out}	P_{out}	η
200	**15**	**0,95**	**14,25**	**17,5**	**0,78**	**13,65**	**95,7**
600	**16**	**2,6**	**41,6**	**17,5**	**2,3**	**40,25**	**96,8**
1000	**17,2**	**4,5**	**77,4**	**17,5**	**4,3**	**75,25**	**97,2**

When the solar irradiation is 1000 W/m^2, the input voltage that is coming from the PV panel has a value of 17.2*V* and the current from the PV panel has a value of 4.5*A*, therefore, the input power has a value of 77.4*W*. While the output voltage value of the PV panel is *17.5V*, the output current value *is* 4.3*A*, therefore, the output power is 75.25*W*, and the percentage efficiency is 97.2.

The calculated values show that the MPPT circuit enhances the power extraction capability of the load by tracking MPP quickly using STM32 Microcontroller. Also, the designed (*P* and *O*) conductance algorithm is very useful and accurate.

CHAPTER 5

CONCLUSIONS AND FUTURE RESEARCH

To exploit all power of photovoltaic (PV) system and maximize the efficiency system, it is necessary to track the maximum power point of the input source. In this research work, the efficiency of perturb and observe (*P* and *O*) maximum power point tracker (MPPT) has been enhanced. A comparison of the normal PV system is done when the modified MPPT. Both the circuits are studied for different values of radiation. Output power at load, the maximum power that solar module can produce are computed in three different cases, and the efficiency is calculated. It is observed that the power efficiency is increased by applying the modified MPPT circuit and the load is able to extract maximum power with high efficiency. Although due to converter circuit and other circuitry power loss increased but still this method is very useful and efficient as a whole while dealing with high power rating modules, where we can ignore the circuitry losses.

5.1 Synopsis

An updated algorithm has been studied in this work to optimize and develop tracking of the highest energy point in a PV framework. A modified method for determining and refreshing the duty cycle (as reference) has been also studied and analyzed. The proposed algorithm has been developed to handle the variation of climate and irradiation that results in loses of energy. Details about solar panel, their properties, and electrical features have been discussed at first chapter.

Particularly, the solar panel's outcome energy *Po* has been explained according to the solar panel's outcome voltage V_p and outcome current I_p. Beginning from the properties of solar panels, MPPT features and it's crucially is highlighted in details. Consequently, the most popular topics which affect negatively on MPPT were classified. A lot of current algorithms that contains the most common algorithms have been debated at second chapter. Furthermore, previous studies that represented real efforts to improve the MPPT algorithms were discussed as well.

At third chapter better and updated algorithm has been present, to optimize and develop tracking of the highest energy point in a PV framework. The designed algorithm was developed to handle the troubles of variant insolation levels and the effect of fluctuation in MPP vicinity. Further, STM microcontroller was included in PCB design of MPPT algorithm to give more improvements. An updated method was mentioned and explained to determine and refresh the duty cycle (as reference). In this way, we can define the action point with greater accuracy and sensitivity. Therefore, the experimental outcomes and simulation computer program results have been manifested to verify the efficiency and improvements of designed algorithm. All details and factors of proposed design regarding to simulation test was done via simulation computer program environment.

The efficiencies and temporary/permanent responds of designed and normal algorithm was compared and analysed, where the comparison has been applied on various simulation computer program environments and radiations levels such as (*200, 500,* and *1000*)*W/m*. To explain the degree of improvement and development for temporary/permanent responds different figures and tables were shown for both algorithms. The hardware implementation prototype has been implemented using STM microcontroller, boost converter and solar panel (*80 W*).

5.2 Future Study

The proposed algorithm has been designed according to boost converter's properties. To make more enhancements and improvements, these rules of updating reference may be tested on other algorithms too. Furthermore, this algorithm may be used with grid off solar panel systems, to support the charging of battery. The STM microcontroller gives more abilities and choices to improvements. In addition, the capabilities of applying on single or triple phase solar systems (grid-on or grid-off systems). To support the results of experimental test, developed simulator instrument of solar panels can be used in the future. Because, these kinds of simulators give the ability to handle variations caused by climate change. The designed algorithm with all electronic circuit could be comprehensively upgraded to create end user device with multiple choices for various solar panel power types.

REFERENCES

[1] U.S. Department of Energy. Energy Efficiency and Renewable energy. History of Solar. Available at: https//www1.eere.energy.gov/solar/pdfs/ solar_timeline.pdf. Accessed 17.04.2019.

[2] Turhan, K. (2011). Fotovoltaik Modüller için Bir Gerçek Saha Performans Ölçüm Platformunun Tasarımı, Kurulumu ve Testleri. Available at: http://hdl.handle.net/11527/12786. Accessed 21.06.2019.

[3] Climate Technology Centre and Network. Solar PV Technology Fact Sheet.

[4] Barutcu, B. (2015- 2016). Bahar Yariyil; Fotovoltaik Güç Sistemleri I.T.U. Energy Institute, Istanbul.

[5] Fraunhofer Institute. (2018). Photovoltaics Report. Fraunhofer Institute for Solar. Energy Systems ISE, Freiburg. Available at: https://www.ise.fraunhofer.de/content/dam/ise/de/documents/publications/studies/Photovoltaics-Report.pdf. Accessed 22.07.2020.

[6] Lynn, P.A. (2010). *Electricity from sunlight: An introduction to photovoltaics*, John Wiley & Sons, 238 p.

[7] Markvart, T. (2000). Solar electricity, Wiley.

[8] Jallad, J. Design and simulation of a photovoltaic system with maximum power control to supply a load with alternating current.

[9] Alsayid, B. (2012). Modelling and Simulation of Photovoltaic Cell/Module/Array with Two Diode Model. *International Journal of Computer Technology and Electronics Engineering*, 1(3**)**, 611.

[10] Luque, A., Hegedus, S. (2003). Handbook of Photovoltaic Science and Engineering. Wiley, 1st ed, west Sussex, UK.

[11] Koutroulis, E., Kalaitzakis, K., Voulgaris, N. C. (2001). Development of a microcontroller-based, photovoltaic maximum power point tracking control system. *IEEE Trans. Industrial Electronics,* **53**, 46-54.

[12] Souza, N. S., Lopes, L. A. C., Liu, X. J. (2005). An intelligent maximum power point tracker using peak current control. *IEEE Power Electronic Specialists PESC Conference,* 172-177.

[13] Petrone, N. G., Spagnuolo, G., Vitelli, M. (2005). Optimization of perturb and observe maximum power point tracking method. *IEEE Trans. Power Electronics,* **20(4),** 963-973.

[14] Leyva, R., Alonso, C., Queinnec, L., Pastor, A. C., Lagrange, D., MartinezSalamero, L. (2006). MPPT of photovoltaic systems using extremum- seeking control. *IEEE Trans. Aerospace and Electronic Systems*, 42, 249-258.

[15] Lee, D., Noh, H., Hyun, D., Choy, I. (2003). An improved MPPT converter using current compensation method for small scaled PV Applications. *IEEE Applied Power Electronics Conf. and Exposition*. **1,** 540-545.

[16] Won, C., Kim, D., Kim, S., Kim, W. A., Kim, H. A. (1994). New maximum power point tracker of photovoltaic arrays using fuzzy controller. *IEEE Power Electronics Specialists Conference*, **1,** 396-403.

[17] Ko, J., Jung, B., Park, K., Choi, C., Chung, D. (2008). Maximum power point tracking control of PV system for DC motors drive with neural networks. *IEEE Smart Manufacturing Application International Conf.,* 514-519.

[18] Xiao, W., and Dunford, W. G. (2004). A modified adaptive hill climbing MPPT method for photovoltaic power systems. *IEEE Power Electronics Specialists Conf*. 1957-1963.

[19] Liu, F., Duan, S., Liu, F., Liu, B., Kang, Y. (2008). A variable step size INC MPPT method for PV systems. *IEEE Trans. Industrial Electronics,* **55(7),** 2622-2628.

[20] Abdelsalam, A.K., Massoud, A.M., Ahmed, S., Enjeti P. (2011). High-performance adaptive perturb and observe MPPT technique for photovoltaic-based microgrids. *Power Electron, IEEE Trans*, **26**, 1010–1021.

[21] Sera, D., Teodorescu, R., Hantschel, J., Knoll M. (2008). Optimized Maximum Power Point Tracker for fast changing environmental conditions. *Industrial Electronics, ISIE 2008 IEEE International Symposium*, 2401–24077.

[22] Mohan, N., Undeland, T. M., Robbins, W. P. (2002). Power Electronics: Converters, Applications, and Design, 3rd ed., Wiley.

[23] Sankarganesh, R., Thangavel, S. (2012). Maximum power point tracking in PV system using intelligence based P and O technique and hybrid cuk converter. *2012 International Conference on Emerging Trends in Science, Engineering and Technology IEEE (INCOSET)*, 429-436.

[24] Souza, N., Opez, N. L., Liu, X. (2006). Peak current control based maximum power point trackers for faster transient responses. IEEE Canadian Conf. on Electrical and Computer Eng. Canadian Conf. CCECE, 659-663.

[25] Samangkool, K., Premrudeepreechacharn, S. (2005). Maximum power point tracking using neural networks for grid-connected photovoltaic system. *IEEE Future Power Systems International Conf*, 1-4.

[26] Mutoh, N., Ohno, M., Inoue, T. (2006). A method for MPPT control while searching for parameters corresponding to weather conditions for PV generation systems. *IEEE Trans. Industrial Electronics*, **53(4)**, 1055-1065.

[27] Lee, J., Bae, H., Cho, B.H. (2006). Advanced incremental conductance MPPT algorithm with a variable step size, Proc. *IEEE Power Electronics and Motion Control Conf*., 603-607.

CV

Muhammed Akil RIHAVI, has Syrian and Turkish Nationalities.

EDUCATION:

- BCs (Eng.) second class honor in Electronic Engineering, Medical Electronic Engineering Department. Faculty of Electrical & Electronic Engineering, University of Aleppo, Aleppo (Syria).
- MSc Degree, Gaziantep University, Gaziantep (Turkey).

LANGUAGES:

- Mother Tongue: Arabic.
- Foreign Languages: English (TOEFL PBT), Turkish (TOMER).

WORK EXPERIENCE:

- **3/6/12–5/10/12** Electronics engineering technician, BIB Tex, Aleppo (Syria).
- **3/6/13–5/7/14** Administration department manager, Ahl-Alkhair Association, Aleppo (Syria).
- **15/1/16–5/7/16** Electrical equipment assembler, Yilkar Klima, Bursa (Turkey).
- **18/8/17–7/6/18** Electrical engineer, Solarturk Enerji, Gaziantep (Turkey).
- **10/6/18 14/2/19** Sales and marketing department manager, ENERGCO, Gaziantep (Turkey).
- **1/4/19–Present** Foreign Trade Coordinator, IPEK MEKIK CARPET, Gaziantep (Turkey).